Science of the Total Environment 621 (2018) 1124–1141

Contents lists available at ScienceDirect

Science of the Total Environment

journal homepage: www.elsevier.com/locate/scitotenv

Flood susceptibility assessment in Hengfeng area coupling adaptive neuro-fuzzy inference system with genetic algorithm and differential evolution

Haoyuan Hong [a,b,c], Mahdi Panahi [d], Ataollah Shirzadi [e], Tianwu Ma [a,b,c], Junzhi Liu [a,b,c], A-Xing Zhu [a,b,c,*], Wei Chen [f], Ioannis Kougias [g], Nerantzis Kazakis [h]

[a] Key Laboratory of Virtual Geographic Environment, Nanjing Normal University, Nanjing 210023, China
[b] State Key Laboratory Cultivation Base of Geographical Environment Evolution (Jiangsu Province), Nanjing 210023, China
[c] Jiangsu Center for Collaborative Innovation in Geographic Information Resource Development and Application, Nanjing, Jiangsu 210023, China
[d] Young Researchers and Elites Club, North Tehran Branch, Islamic Azad University, Tehran, Iran
[e] Department of Rangeland and Watershed Management, Faculty of Natural Resources, University of Kurdistan, Sanandaj, Iran
[f] College of Geology and Environment, Xi'an University of Science and Technology, Xi'an 710054, China
[g] European Commission, Joint Research Centre (JRC), Directorate for Energy, Transport and Climate, Italy
[h] School of Geology, Aristotle University of Thessaloniki, Greece

HIGHLIGHTS

- ANFIS was coupled with GA and DE for flood susceptibility modelling.
- 195 flood events were used for the ANFIS training.
- SWARA method was used to evaluate the relationship between floods and conditioning factors.
- ANFIS-DE model shows the better result in flood prediction.
- Very high flood susceptible area is up to 20 km^2

GRAPHICAL ABSTRACT

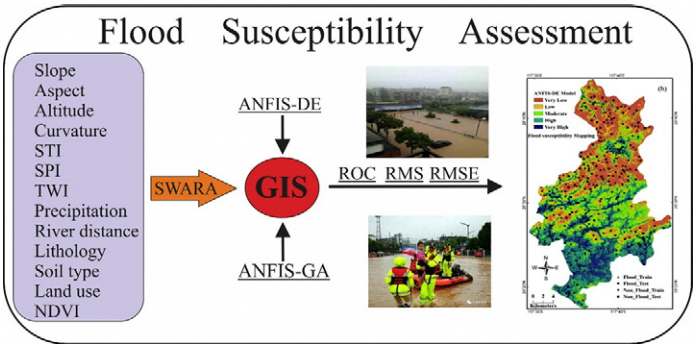

ARTICLE INFO

Article history:
Received 6 September 2017
Received in revised form 4 October 2017
Accepted 12 October 2017
Available online 1 November 2017

Editor: Wei Ouyang

Keywords:
Climate change
Flood susceptibility
ANFIS
Genetic algorithm

ABSTRACT

Floods are among Earth's most common natural hazards, and they cause major economic losses and seriously affect peoples' lives and health. This paper addresses the development of a flood susceptibility assessment that uses intelligent techniques and GIS. An adaptive neuro-fuzzy inference system (ANFIS) was coupled with a genetic algorithm and differential evolution for flood spatial modelling. The model considers thirteen hydrologic, morphologic and lithologic parameters for the flood susceptibility assessment, and Hengfeng County in China was chosen for the application of the model due to data availability and the 195 total flood events. The flood locations were randomly divided into two subsets, namely, training (70% of the total) and testing (30%). The Step-wise Weight Assessment Ratio Analysis (SWARA) approach was used to assess the relation between the floods and influencing parameters. Subsequently, two data mining techniques were combined with the ANFIS model, including the ANFIS-Genetic Algorithm and the ANFIS-Differential Evolution, to be used for flood spatial modelling and zonation. The flood susceptibility maps were produced, and their robustness was checked using the Receiver Operating Characteristic (ROC) curve. The results showed that the area under the curve (AUC) for all models was >0.80. The highest AUC value was for the ANFIS-DE model (0.852), followed by ANFIS-GA (0.849). According to the

* Corresponding author at: Key Laboratory of Virtual Geographic Environment, Nanjing Normal University, Nanjing 210023, China.
E-mail addresses: hong_haoyuan@outlook.com (H. Hong), azhu@wisc.edu (A.-X. Zhu).

https://doi.org/10.1016/j.scitotenv.2017.10.114

Differential evolution
Hengfeng County

RMSE and MSE methods, the ANFIS-DE hybrid model is more suitable for flood susceptibility mapping in the study area. The proposed method is adaptable and can easily be applied in other sites for flood management and prevention.

1. Introduction

The significance of water is well documented in the Chinese tradition through quotations such the one by the philosopher Laozi, who praises the importance of water: "The best of men are like water; water benefits all things". Nonetheless, flood incidents are extreme water flow events with often catastrophic consequences. Floods are considered a natural hazard, and they cause major economic losses and seriously affect peoples' lives and health globally (Dottori et al., 2016). According to the United Nations Office for Disaster Risk Reduction (UNISDR), between 1996 and 2015, the number of casualties due to flood events was 150,061 globally, representing 11.1% of the global disaster mortality.

Flood occurrence is a complex and site-dependent phenomenon that has always intrigued scientists, compelling them to explore, analyse and better understand its mechanisms. Robins et al. (2009) defined surface stability, vegetation, soil growth, and diagnostic horizon data as the key factors for flood disaster evaluation (Robins et al., 2009). The reasons for flood occurrence and development can be distinguished between human and natural factors. Climate change is considered an important factor for extreme flood/drought occurrence (Rojas et al., 2012; Sampson et al., 2015). In that sense, Charlton et al. (2006) claimed that climate-induced alterations may influence land use and eventually increase flood risk, as the additional impermeable surfaces, drains and sewers favour rapid water transfer. Increased flow speed reduces the available response time and further increases the volume of the peak flow (Charlton et al., 2006). Arnell and Gosling (2016) evaluated the impact of climate change on global river flood risk, demonstrating that the latter would increase by approximately 187% by 2050, with Asia expected to be the most affected (Arnell and Gosling, 2016). Emerton et al. (2017) compared El Niño and La Niña events, which are also often grouped together under the term El Niño Southern Oscillation (ENSO). The extremes of the ENSO climate variability appear to influence river flow and flood recurrence at a global scale (Emerton et al., 2017). In their research, Wang et al. (2015) analysed the maximum values for 3-day precipitation, typhoon frequency and runoff depth as indices of flood development (Wang et al., 2015). The need to include additional parameters for rainfall accumulation is a widely accepted approach, as rainfall accumulation is a required but insufficient condition for inducing flash floods (Norbiato et al., 2008), as local hydrology critically controls flash flood creation. Initial soil moisture is an additional important factor, as is human intervention. The removal of vegetation results in soil erosion. Uncontrolled waste disposal minimizes the river's capacity and exacerbates the flood hazard. Urbanization also increases the flood risk as a major force altering the hydrological processes over a range of temporal and spatial scales (Suriya and Mudgal, 2012).

As stated by Dobler et al. (2012), flood susceptibility is a prerequisite for sustainable flood risk management, as it provides useful information about the appropriate strategies for adaptation and mitigation (Dobler et al., 2012). Flood susceptibility assessment generally builds on the latest Geographic Information System (GIS) tools to process and analyse complex planning strategies, decision making, and integrated management. GIS integrates maps in a visual manner that is query-based with statistical analyses. This explains its wide use in environmental management and modelling, including landslides, forest fires and flood hazards (Xiao et al., 2017). GIS has facilitated flood susceptibility studies and significantly improved their accuracy (Nunes Correia et al., 1998). The various parameters related to flood susceptibility may be used through heuristic approaches by assigning different weights depending on their relative importance. However, the recent practice of flood susceptibility modelling promoted statistical techniques via univariate or multivariate models, as they are considered more objective quantitative methods (de Walque et al., 2017).

In the current literature, one can find three main types of flood susceptibility assessment: i) hydrological models such as HYDROTEL (Aissia et al., 2012), SWAT (Oeurng et al., 2011), and WetSpa (Bahremand et al., 2007); ii) statistical and data-driven approaches such as the analytic hierarchy process (AHP) (Kazakis et al., 2015; Stefanidis and Stathis, 2013), frequency ratio (FR) (Tehrany et al., 2015a), logistic regression (LR) (Ettinger et al., 2016; Nandi et al., 2016), weights-of-evidence (WOE) (Tehrany et al., 2014a), and fuzzy logic (FL) (Pulvirenti et al., 2011); and iii) non-linear machine learning algorithms such as artificial neural network (ANN) (Kia et al., 2012), decision tree (DT) (Tehrany et al., 2013a), support vector machine (SVM) (Tehrany et al., 2015c), k-nearest neighbor (KNN) (Liu et al., 2016), and random forest (Wang et al., 2015). The aforementioned methods have successfully provided flood susceptibility assessments, but they also face some limitations (Ward et al., 2015). For example, conventional hydrological models are not robust automated methods because the model design, building and parameter calibration is time consuming. Statistical and data-driven methods have an increased subjectivity as they require selecting the flood conditioning factors. Chen et al. (2015) applied a multicriteria decision analysis method to evaluate flood hazard in Japan and observed that low-quality data may lead to errors and low-quality results (Chen et al., 2015). In the process of modelling, non-linear machine learning algorithms may also lead to poor projections due to the large and inconsistent value ranges in the datasets (Tien Bui et al., 2016a).

Although flooding is a serious hazard for China, insufficient attention has been paid to flood hazard assessment. Winsemius et al. (2016) coupled climate, socio-economic and hydrologic models to research global future river flood risk. The result showed that countries in Southeast Asia may face increased flood risk, especially in the Yangtze river (Winsemius et al., 2016). Human life and economic losses in China have been significant throughout history (Zong and Chen, 2000). Yu et al. (2009) analysed historical floods on the Yangtze River, China and concluded that after 1950, the flood frequency increased and that anthropogenic activity (e.g., deforestation, diking, and lake-coast reclamation) is an important factor for flooding (Yu et al., 2009).

This paper investigates the main influencing factors for flood susceptibility in the Hengfeng area, China. Climate change, local geomorphology, topography and hydrology are analysed, along with human activities and intervention. Accordingly, the analysis aims to identify the key factors in flood susceptibility modelling. A GIS-based model has been developed to perform flood susceptibility mapping in Hengfeng County, China. It is coupled with a neuro-fuzzy inference system (ANFIS) that incorporates a genetic algorithm (GA) and differential evolution (DE) models while comparing their performance. The main difference between the proposed methodology and existing studies is the coupling of ANFIS to GA and DE, which –to the authors' knowledge – is implemented for the first time. The overall performance of the models was evaluated using the appropriate datasets and collected information. Root Mean Square Error (RMSE), Mean Absolute Error (MAE), Receiver Operating Characteristic (ROC) curve, and area under the ROC curve (AUC) evaluated the model performance. High risk locations for flood and the projected magnitude and distribution of the flood hazard can support governmental planning and decision makers' work on devising flood management mitigation strategies and planning (Xiao et al.,

2017). Finally, the robustness of the model was evaluated by comparing the flood susceptibility map with historical flood events.

2. Data and methods

The developed methodology follows the following five steps: i) selecting the study area; ii) data assembly, including collecting the flood inventory map and influencing factors; (iii) factor correlation using Step-wise Weight Assessment Ratio Analysis (SWARA); (iv) flood spatial modelling using the ANFIS-GA, and ANFIS-DE models; and (v) validation and model comparison (see Fig. 1).

2.1. Description of the study area

Hengfeng County covers an area of approximately 655 km^2, located in Jiangxi Province, China. The region lies at a longitude of 117°29′11″ to 117°46′30″E and a latitude of 28°17′20″ to 28°44′00″N (Fig. 2). The elevation of Hengfeng County varies from −41 to 1347 m (msl).

2.1.1. Climate

The climate of the Hengfeng area is subtropical monsoon. According to the report from the Jiangxi meteorology bureau (http://www.weather.org.cn/), the average temperature from 1959–2003 is 18.3 °C, and the humidity is 76%. The average annual sunshine duration is 76.6 days, and the average maximum wind speed is 2.1 m/s. The average number of rainy days is 122 d, with an average annual rainfall of 1882.1 mm. Due to the monsoon and the geographical position, rainfall is unevenly distributed both in time and space; the maximum annual rainfall is 2864.2 mm, but the minimum annual rainfall of 1079.8 mm, which is 2.65 times lower. The annual distribution of rain is also uneven, with 60% of the annual precipitation concentrated between April and July. The north region receives more precipitation than does the southeast, and in the records of several years, the maximum daily rainfall appears in June as a torrential rainstorm, with an average height of 255.3 mm.

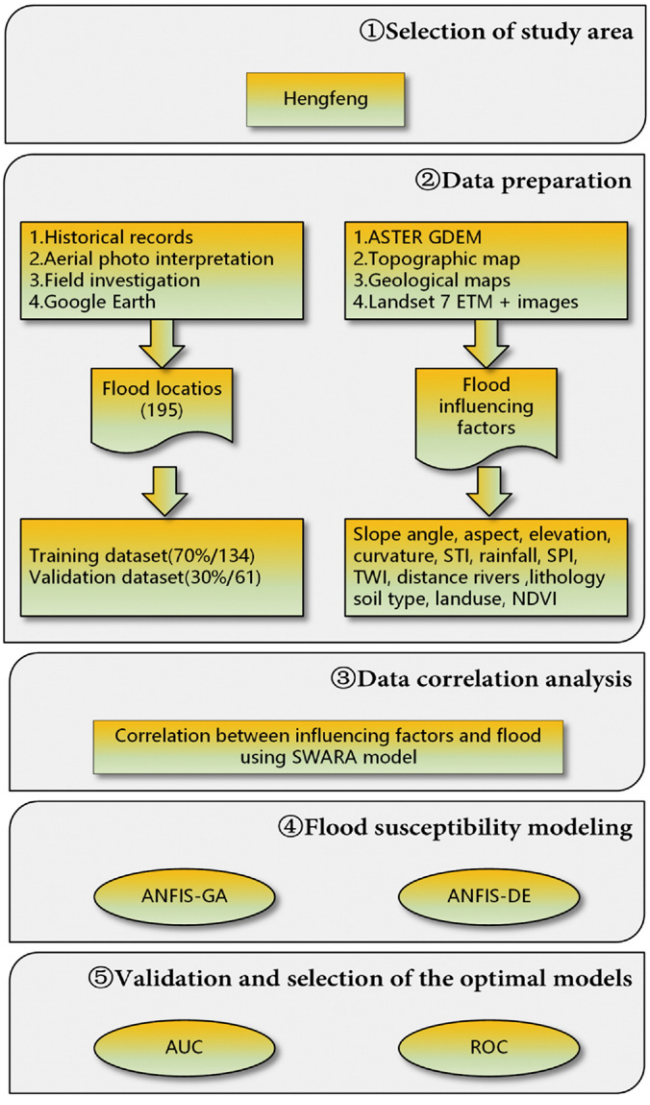

Fig. 1. Flowchart of the developed methodology.

2.1.2. Hydrology

The Hengfeng river basin belongs to the Poyang water system, and the five major rivers in the Hengfeng County are the Gexi river, Ceng ganghe river, Gangbian river and Wei huangcun river. Over the past several decades, the study area has been hit by floods several times.

2.1.3. Geology and soil

Analysing the geological map of Hengfeng County, it appears that the area hosts >29 geologic groups and units, with the main lithology being basalt, rhyolite, lava, syenite and pyroxene amphibolite (a map and table are in the supplementary information).

2.1.4. Population and economy

The population of Hengfeng County is 184,870 people, with 74,262 of them living in towns (40.17%) and 110,608 living in rural areas (59.83%). The Gross Domestic Product (GDP) of Hengfeng County is approximately 1 billion US dollars per year.

2.1.5. Flood event

The heavy rainfall is the main factor for floods, according to a recent report of the Hengfeng government (http://zfxx.hfzf.gov.cn) and historical records. The most destructive events occurred in Jun 1964, Jun 1971, Aug 1997, Jun 1998 and Jun 1999. In particular, in 1998 (June 12 to 21), the total rainfall was approximately 930.3 mm, and persistent rainstorms outreached the natural drainage capacity. Approximately 100,000 people were affected, the area of flooded crops was 55 km^2, 12,800 houses were damaged, 229 km of road network was damaged, and 287 bridges and 128 dams were damaged. Communications were interrupted in 9 towns, and the direct economic loss was approximately 20 million US dollars.

2.2. Data preparation

2.2.1. Flood inventory map

The first step of the developed methodology is to create a flood inventory map by collecting information on historical flood events, processing aerial photos, performing field investigations and analysing remote sensing datasets (Santangelo et al., 2011). Historical records of floods may have limited spatial and temporal accuracy due to land use changes. Thus, it may add uncertainty to the results (Hagen et al., 2010). Rashid (2011) used newspaper articles as a source of flood information to understand the extent of flood events (Rashid, 2011). Ho and Umitsu (2011) utilized Shuttle Radar Topographic Mission (SRTM) and LANDSAT ETM + (Enhanced Thematic Mapper Plus) data to analyse the flood hazard on the Thu Bon alluvial plain, in central Vietnam. The result showed the efficacy of satellite data in replacing topographic and land cover data, where available (Ho and Umitsu, 2011).

The present study, combining the mentioned approaches and the flood inventory map for the Hengfeng area, was prepared using a collection of historical information on individual flood events, interpretation of aerial photographs, and high-resolution image processing. The sources of this information were the department of civil affairs of Jiangxi Province (http://www.jxmzw.gov.cn/), the Jiangxi meteorological

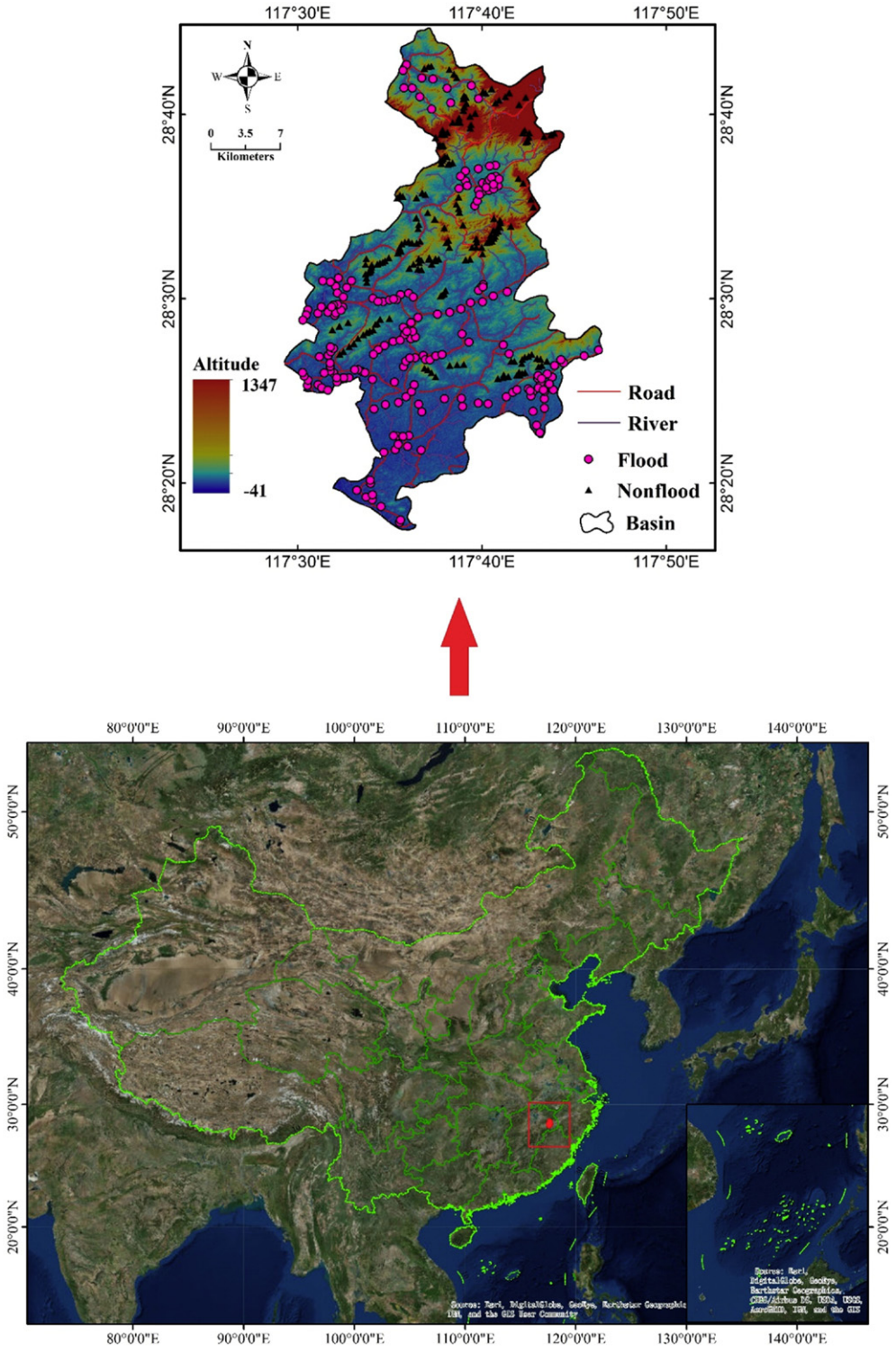

Fig. 2. The study area and spatial distribution of floods.

bureau (http://www.weather.org.cn/) and the ministry of water resources of Jiangxi Province (http://www.jxsl.gov.cn/).

Eventually, 195 flood events were mapped in the study area (Fig. 2). These records were divided into two subsets, namely, training and testing (70/30), based on a random selection method. The training data, consisting of 70% or 134 events, was used to train the models, whereas testing data (30%, 61 events) were used for model validation. Fig. 2 in the Supplementary information shows some photos about the flood events in Hengfeng County.

2.2.2. Flood influencing factors

Several factors contribute to flooding including natural factors and human activities (Youssef et al., 2011). Slater et al. (2015) showed that

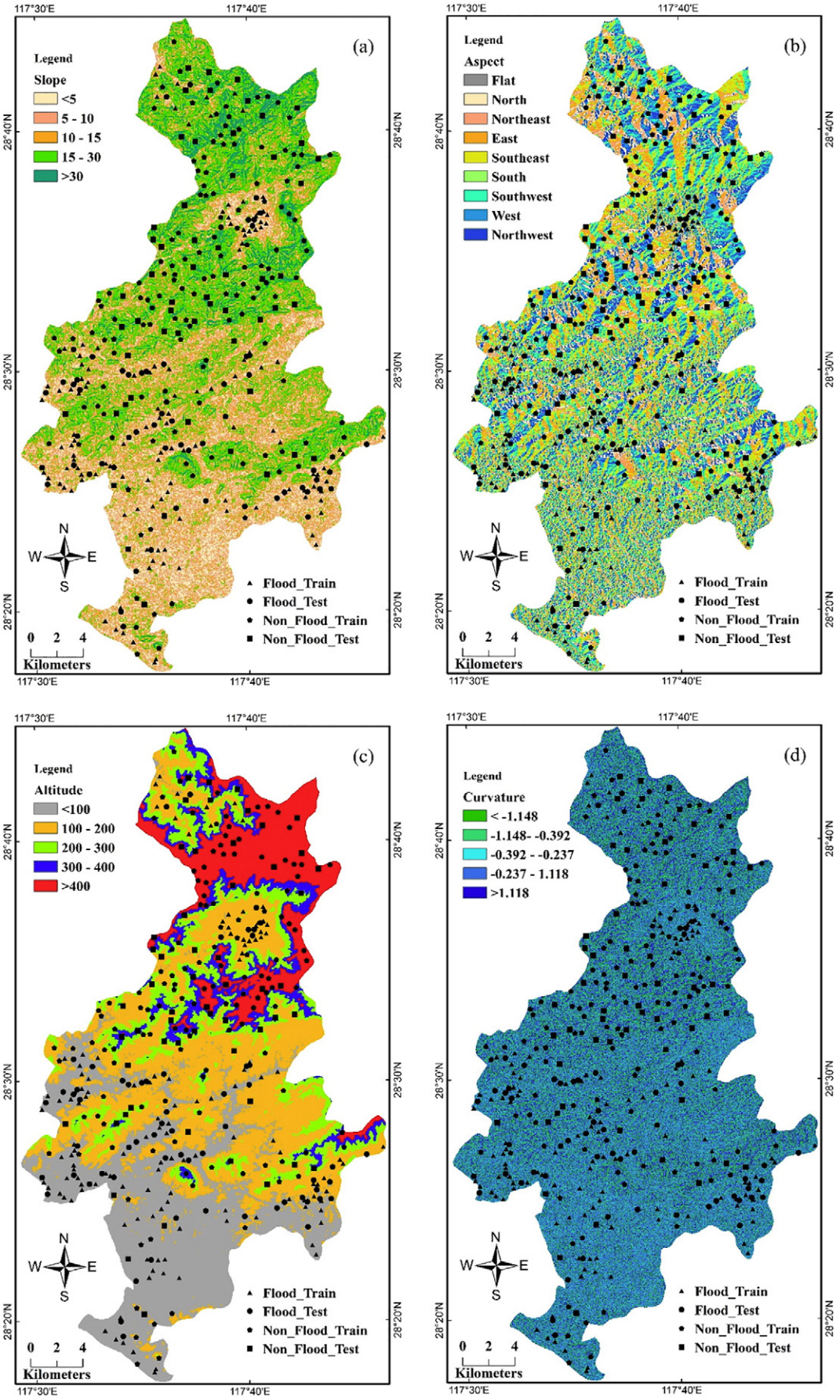

Fig. 3. Flood conditioning factor a) Slope, b) Aspect, c) Altitude, d) Curvature, e) STI, f) SPI, g) TWI, h) Rainfall, i) Distance to rivers, j) Lithology, k) Soil, l) Land use, m) NDVI.

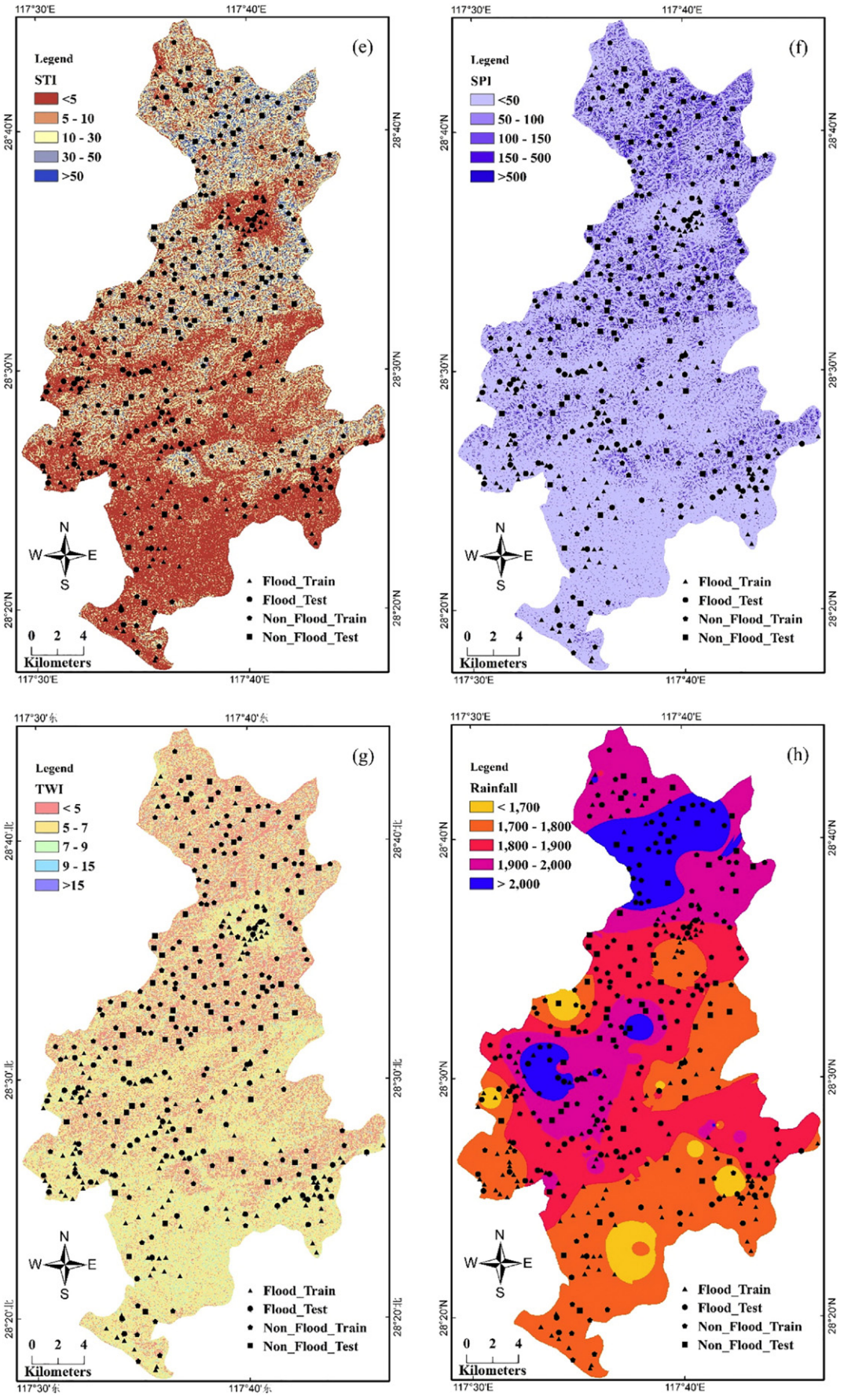

Fig. 3 (*continued*).

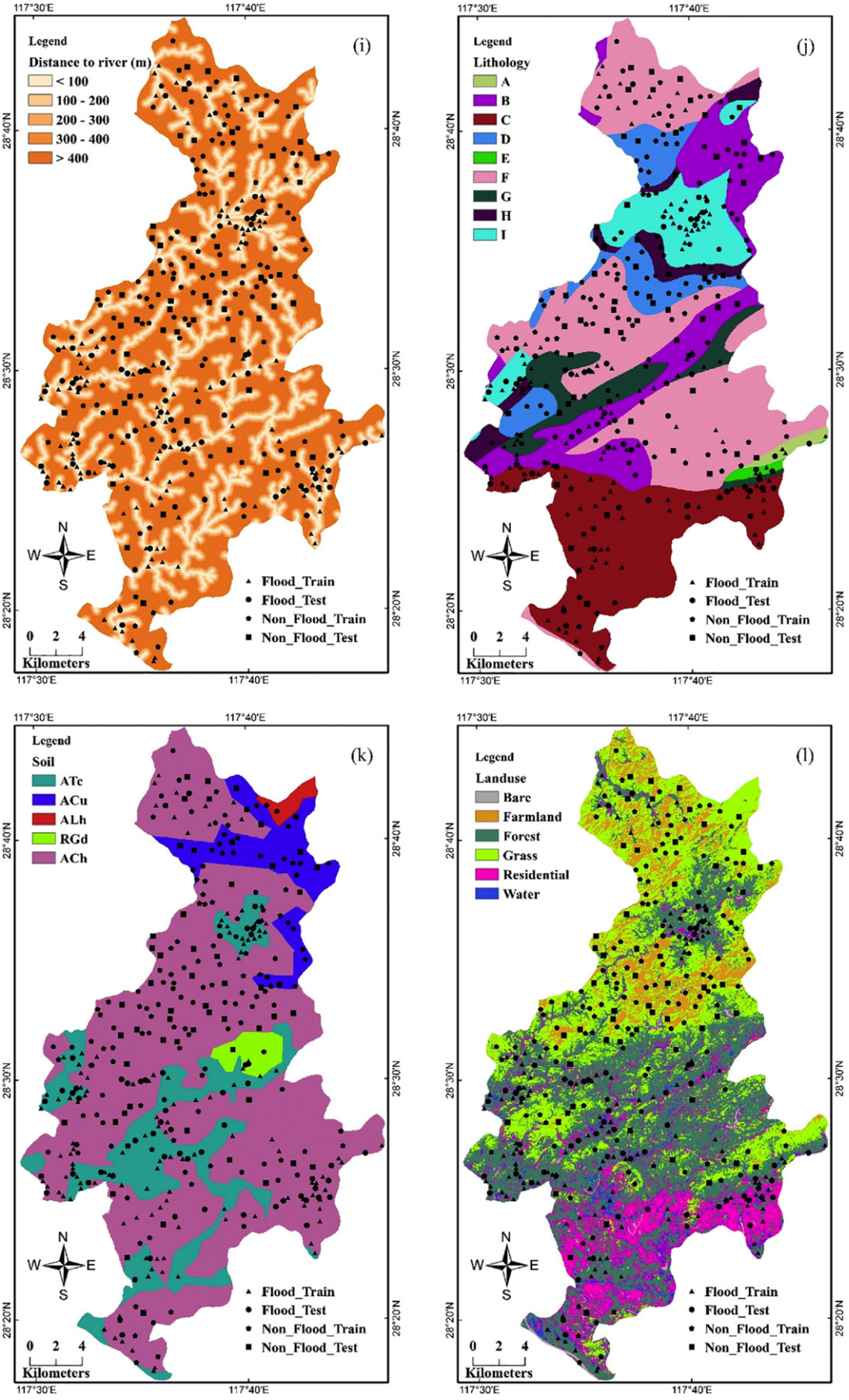

Fig. 3 (*continued*).

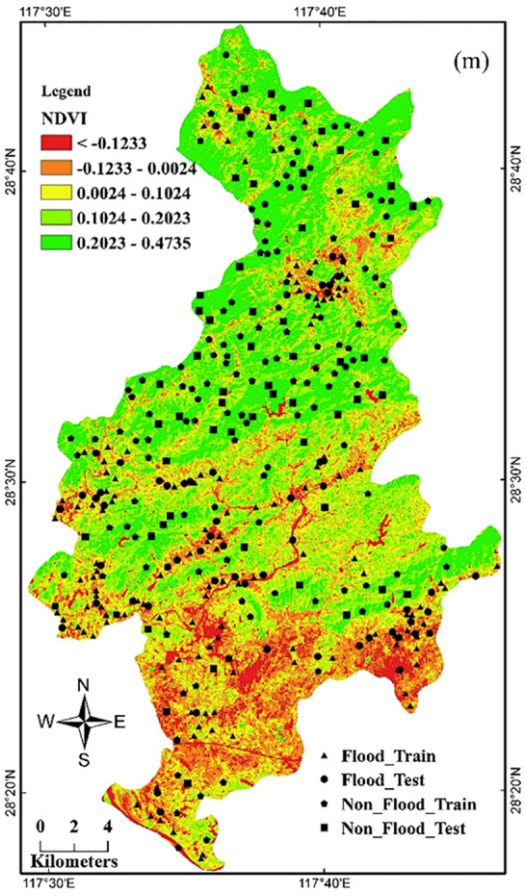

Fig. 3 (*continued*).

geomorphology is a common flood hazard driver and may be more common – but less significant – than hydrology (Slater et al., 2015).

The present study analysed thirteen influencing factors: slope, aspect, altitude, curvature, the sediment transport index (STI), the stream power index (SPI), the topographic wetness index (TWI), rainfall, distance to rivers, lithology, soil type, land use and the normalized difference vegetation index (NDVI). The spatial distribution of all 13 factors is illustrated in Fig. 3. Data analysis and visualization were performed in the GIS environment, with the data having a raster format and spatial resolution of 30 m, and the classes of all parameters were determined according to the corresponding literature.

2.2.2.1. Slope. The water velocity is determined by the slope gradient; therefore, slope is an important factor for flood susceptibility (Fernández and Lutz, 2010). Water flows from higher to lower elevations, so the slope influences the amount of surface runoff and infiltration. Flat areas at low elevations may flood more quickly than areas at higher elevations with a steeper slope (Kazakis et al., 2015). Li et al. (2012) also stated that the possibility of flood occurrence is relatively higher in areas with smaller slopes (Li et al., 2012). Slope is also relevant for downstream changes, as shown in stream power models and the longitudinal distribution of river floods (Barker et al., 2009). Çelik et al. (2012) concluded that high slopes may accelerate precipitation transformation into runoff (Çelik et al., 2012). In the present study, slope was distinguished into 5 categories: (1) 0–5; (2) 5–10; (3) 10–15; (4) 15–30; and (5) 30–71.375.

2.2.2.2. Aspect. Yates et al. (2000) analysed the flash flood in Buffalo Creek watershed, with the results showing that aspect is an important parameter in hydrologic response units (Yates et al., 2000). Hydrologic processes, local climatic conditions, physiographic trends and soil moisture patterns are affected by aspect (Rahmati et al., 2016). Gutiérrez-Jurado et al. (2007) used the differential responses of slopes to a major flood event in a semiarid catchment, and the results demonstrated that aspect has an indirect effect on the channel flood (Gutiérrez-Jurado et al., 2007). In the present study, aspect was distinguished into 9 categories: 1) Flat; (2) North; (3) Northeast; (4) East; (5) Southeast; (6) South; (7) Southwest; (8) West; and (9) Northwest.

2.2.2.3. Altitude. Li et al. (2012) explored the possible relationship between various factors and flood occurrence. The results of the analysis showed that lower altitude is prone to flooding (Li et al., 2012). Altitude also has a significant influence on flood regulation functions, as there is a clear trend of increased precipitation and river discharge with increasing altitude (Nedkov and Burkhard, 2012). In the present study, altitude was distinguished into 5 categories: (1) <100; (2) 100–200; (3) 200–300; (4) 300–400; and (5) 400–1347 m.

2.2.2.4. Curvature. Hudson and Kesel (2000) studied the relationship between curvature and floods in the lower Mississippi River, concluding that curvature between 1.0 and 2.0 is sensitive to flooding (Hudson and Kesel, 2000). Curvature affects the heterogeneity and hyporheic flow, including bed forms and water surface topography (Cardenas et al., 2004). As curvature supports projections on water depths and model calibration, its inclusion is beneficial for the accurate representation of velocity (Horritt, 2000). In the present study, curvature was distinguished into 5 categories: (1) [(−16.88)–(−1.148)]; (2) [(−1.148)–(−0.392)]; (3) [(−0.392)–(−0.237)]; (4) [(−0.237)–1.118]; and (5) [1.118–15.222].

2.2.2.5. Sediment transport index (STI). The estimation of the STI index is performed with Eq. (1):

$$\mathrm{STI} = \left(\frac{A_s}{22.13}\right)^{0.6}\left(\frac{\sin\beta}{0.0896}\right)^{1.3} \quad (1)$$

where β represents the slope at each pixel and A_s represents the upstream area (Moore et al., 1991). The occurrence and intensity of erosion and sediment transport depends on the hydroclimatic and geomorphologic characteristics of the basin, together with the availability of sediment within the catchment (López-Tarazón et al., 2010). The sediment transport index is directly associated with sediment accumulation and changes in channel bed elevation, structures and navigation systems (Naik and Jay, 2011). Billi (2011) claimed that sediment dynamic processes may increase flood frequency and result in foundation damage (Billi, 2011). In the present study, the STI was distinguished into 5 categories: (1) 0–5; (2) 5–10; (3) 10–30; (4) 30–50; and (5) 50–1458.205.

2.2.2.6. Stream power index (SPI). The estimation of the SPI is performed with Eq. (2):

$$\mathrm{SPI} = A_s \tan\beta \quad (2)$$

where A_s represents the specific catchment area and β (radians) represents the slope gradient (Moore et al., 1991). Knighton (1999) found that the stream power index has a significant influence on many processes of the fluvial system (Knighton, 1999). Fuller (2008) analysed the geomorphic impact of a flood in New Zealand, and the result showed that high stream power generated in confined channels resulted in catastrophic channel transformation (Fuller, 2008). The total stream power is the stream capacity to transport sediment and to erode its bed (Troiani and Della Seta, 2008). The stream power index can be defined as a significant performance of fluvial sediment transport, and river channel erosion (Barker et al., 2009). In the present study, the SPI was distinguished into 5 categories: (1) 0–50; (2) 50–100; (3) 100–150; (4) 150–500; and (5) 500–49,279.836.

2.2.2.7. Topographic wetness index (TWI). The estimation of the TWI is performed with Eq. (3):

$$\mathrm{TWI} = \ln(A_s / \tan\beta) \tag{3}$$

where A_s is the cumulative upslope area draining through a point (per unit contour length) and $\tan\beta$ represents the slope angle at the point (Moore et al., 1991). The TWI is a physical attribute of flood-inundation areas, is considered an important parameter of a catchment (Soulsby et al., 2010) and includes two representative measurements: hydrographic position and flat land (Papaioannou et al., 2015). It is used to describe the spatial soil moisture patterns and erosion (Chen and Yu, 2011), and high TWI values are strongly correlated with floodplain development (Adam and David, 2011). In the present study, the TWI was distinguished into 5 categories: (1) 2.365–5; (2) 5–7; (3) 7–9; (4) 9–15; and (5) 15–29.770.

2.2.2.8. Precipitation. There is a large body of previous literature demonstrating the relationship or process between precipitation and flood occurrence (Bouilloud et al., 2010; Goel et al., 2000; Rozalis et al., 2010; Zhang and Smith, 2003). Rainfall is the driver of flood generation (Segond et al., 2007), and its amount is the key factor in flooding, although it is not certain to what extent an increase in rainfall will result in proportionally increased flooding (Kay et al., 2006). Among different regions, annual rainfall was selected as an influencing factor in flood susceptibility mapping (Tehrany et al., 2013a, 2013b; Tehrany et al., 2014a, 2014b; Tehrany et al., 2015a, 2015b, 2015c; Tien Bui et al., 2017). In the present study, annual rainfall was distinguished into 5 categories: (1) 1509.073–1700; (2) 1700–1800; (3) 1800–1900; (4) 1900–2000; and (5) >2000.

2.2.2.9. Distance to a river. Following precipitation events, sediment accumulation occurs when discharge increases, with possible flooding of the surrounding areas (Aalto et al., 2003). Predick and Turner (2008) concluded that river networks play an important role in flood expansion (Predick and Turner, 2008). Previous studies also showed that terrestrial water storage is associated with regional flooding (Antonelli et al., 2008; Reager et al., 2014). In the present study, the distance to a river was distinguished into 5 categories: (1) 0–100; (2) 100–200; (3) 200–300; (4) 300–400; and (5) >400.

2.2.2.10. Lithology. Lithologic variations can affect the stream profile on temporal floods (Reneau, 2000) and is found to be an important factor in the development of floods (Xu et al., 2001). The lithology may also indicate evidence of flood occurrence in geological history (He et al., 2007). In the present study, the lithology was distinguished into 9 categories: (1) A, (2) B, (3) C, (4) D, (5) E, (6) F, (7) G, (8) H and (9) I. The detailed lithology information is in Table 2 in the Supplementary information.

2.2.2.11. Soil type. Soil data are particularly significant for estimating excess precipitation and infiltration (Johnson, 2000). Soil type I is related to local weather conditions and erosion (Flügel, 1995). Infiltration is also strongly determined by the soil properties, and it affects the water balance (Nedkov and Burkhard, 2012) because the soil type also determines the degree of drainage and urbanization (Du et al., 2012). In the present study, soil type was distinguished into 5 categories: (1) ATc (Cumulic anthrosols); (2) ACu (Humic acrisols); (3) ALh (Haplic alisols); (4) RGd (Dystric regosols); and (5) Ach (Haplic acrisols).

2.2.2.12. Land use. Land use changes affect runoff and sediment transport and, as a result, influence flood frequency (Benito et al., 2010). García-Ruiz et al. (2008) demonstrated that land uses are of paramount importance when comparing hydrological responses at different temporal scales (García-Ruiz et al., 2008). Similarly, Beckers et al. (2013) underlined that land use evolution is a key factor for flood risk (Beckers et al., 2013). In the present study, land use was distinguished into 6 categories: (1) Barren land; (2) Grass land; (3) Farm land; (4) Forest land; (5) Water bodies; and (6) Residential areas.

2.2.2.13. Normalized difference vegetation index (NDVI). The estimation of the NDVI index is performed with Eq. (4):

$$\mathrm{NDVI} = \frac{NIR - R}{NIR + R} \tag{4}$$

where the *NIR* represents the infrared portion of the electromagnetic spectrum and *R* represents the red portion of the electromagnetic spectrum. Huang et al. (2012) explored the relationship between the NDVI and flooding in the Dongting area (Huang et al., 2012). The NDVI shows high sensitivity to flood development (Kumar and Acharya, 2016) as it represents different structural features, flood frequency, phenological behaviour and hydro-sedimentology in the floodplain (Marchetti et al., 2016). In the present study, the NDVI was distinguished into 5 categories: (1) [(−0.4712)–(−0.1233)]; (2) [(−0.1233)–(−0.0024)]; (3) [(−0.0024)–(0.1024)]; (4) [(0.1024)–0.2023]; and (5) [0.2023–0.4725].

2.3. Data correlation analysis using the SWARA method

The Step-wise Weight Assessment Ratio Analysis (SWARA) method is a multiple-criteria decision analysis (MCDM) technique for calculating the weight of each criterion. SWARA was presented in 2010 (Keršuliene et al., 2010) and has two main points: First, different situations are analysed, and the criteria are prioritized according to needs and goals. Second, the viewpoint of experts is also considered in SWARA. Experts can play an essential role in the prioritization of criteria (Hashemkhani Zolfani and Bahrami, 2014; Saeidian et al., 2016), a characteristic that resulted in the method's increased application in recent years (Alimardani et al., 2013; Dehnavi et al., 2015; Zolfani et al., 2013). The steps of the method are described in detail in the following text:

Stage one: The experts develop a decision making model based on the relationship between the factors. Then, they prioritize the criteria according to their verdict, and the criteria are sorted in descending order.

Stage two: The weights of the criteria are calculated as follows:

Starting from the second criterion, the respondent expresses the relative importance of the criterion j in relation to the previous $(j-1)$ criterion and repeats for every criterion. According to Keršuliene, this determines the Comparative Importance of the Average Value, S_j, as described in Eq. (5) (Keršuliene et al., 2010):

$$S_j = \frac{\sum_i^n A_i}{n} \tag{5}$$

where n stands for the number of experts; A_i shows the offered ranks by the experts for each factor; and j represents the number of the factor.

Subsequently, the coefficient K_j is determined by Eq. (6):

$$K_j = \begin{cases} 1 & j = 1 \\ S_j + 1 & j > 1 \end{cases} \tag{6}$$

The re-calculated weight Q_j is calculated by Eq. (7):

$$Q_j = \frac{X_{j-1}}{K_j} \tag{7}$$

Eventually, the relative weights of the criteria are calculated by Eq. (8):

$$W_j = \frac{Q_j}{\sum_{j=1}^m Q_j} \tag{8}$$

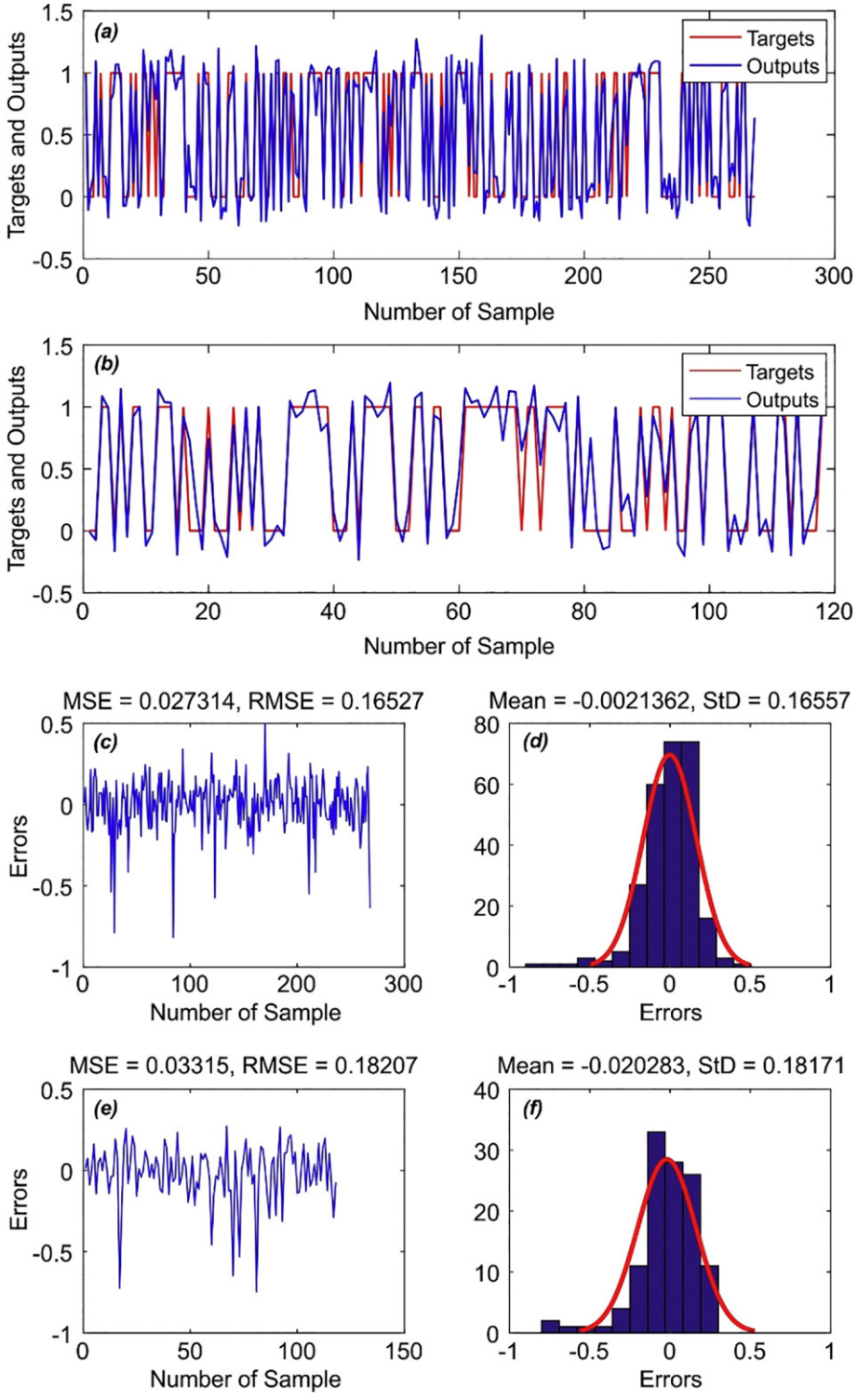

Fig. 4. ANFIS-GA model: a) target and output ANFIS-GA value of train data samples c) MSE and RMSE value of train data samples d) frequency errors of train data samples; b) target and output ANFIS-GA value of testing data samples e) MSE and RMSE value of testing data samples f) frequency errors of testing data samples.

where W_j indicates the relative weight of *j th* criterion and m indicates the total number of the criteria. Details and a flowchart of SWARA method are available in the Supplementary information.

2.4. Flood spatial modelling

2.4.1. Adaptive neuro-fuzzy inference system (ANFIS)

Adaptive Neuro-Fuzzy Inference System (ANFIS) was introduced in 1993 as a combination of the artificial neural network (ANN) and fuzzy logic approaches (Jang, 1993). This hybrid combination aims to create a more reliable structure (Wali et al., 2012) because ANFIS is a data-driven model that has self-learning ability with no input requirements and the fuzzy logic produces the output using fuzzy logical decisions (Mathur et al., 2016; Phootrakornchai and Jiriwibhakorn, 2015). Hence, ANFIS constructs a hybrid intelligent system that can be more efficient than ANN and fuzzy logic (Wali et al., 2012). ANFIS has been widely applied in various domains for solving nonlinear and difficult problems (Rezakazemi et al., 2017), such as environmental data

processing (Jahed Armaghani et al., 2015; Najah et al., 2014), geo-hazard studies (Chau et al., 2005; Chen et al., 2017a; Chen et al., 2017e; Mukerji et al., 2009; Oh and Pradhan, 2011), mining (Asadi et al., 2015), and energy (Onat and Ersoz, 2011). The ANFIS structure contains six layers; two inputs x and y and one output f.

The structure of ANFIS is in Supplementary information, Fig. 4, Structure of ANFIS. A_1,A_2,B_1, and B_2, are the fuzzy sets, and p_i,q_i and r_i are the parameters. Two fuzzy if/then rules are based on Takagi and Sugeno's type (Celikyilmaz and Turksen, 2009) and are considered as follows:

$$\begin{array}{l}\text{Rule 1 : if } x \text{ is } A_1 \text{ and } y \text{ is } B_1, \text{ then } f_{1=}p_1x_+q_1y_+r_1\\ \text{Rule 1 : if } x \text{ is } A_2 \text{ and } y \text{ is } B_2, \text{ then } f_{2=}p_2x_+q_2y_+r_2\end{array} \quad (9)$$

Layer 1 (input layer): the first layer contains the input layer for passing to the neurons of the next layer.

Layer 2 (fuzzification): the fuzzification layer consists of adaptive nodes with A_i and B_{i-2}, which are linguistic labels, and every node calculates the fuzzy membership function (MF), $Q_{1,i}$, for defining a full, none or partial membership level. The output of this layer can be stated in the following equations:

$$\begin{array}{l}Q_{1,i} = \mu_{A_i}(x_1) \quad for \quad i = 1,2\\ Q_{1,i} = \mu_{B_{i-2}}(x_2) \quad for \quad i = 3,4\end{array} \quad (10)$$

Fuzzifying is conducted by membership functions such as the triangular, trapezoidal, Gaussian, and bell functions. Among the abovementioned membership functions, the Bell function is usually used as the membership function because of its smooth and concise notation (Übeyli et al., 2010). Therefore, this paper has used this function as $\mu_{A_i}(x)$, given that

$$\mu_{A_i}(x) = \frac{1}{1+\left\{\left(\frac{x-c_i}{a_i}\right)^2\right\}^{b_i}} \quad (11)$$

where $a_i, b_i, and\ c_i$ are the parameters of the Bell function or so-called premise parameters (Jang, 1993).

Layer 3 (fuzzy AND): The symbol 'M' shows every fixed node in this layer. This layer calculates the firing strength (w_i), and the outputs are computed using the following equation:

$$Q_{2,i} = w_i = \mu_{A_i}(x) \times \mu_{B_i}(y) \quad for \quad i = 1,2 \quad (12)$$

Layer 4 (normalization): Every fixed node (square node) labelled 'N' in this layer is calculated as the ratio of individual rule firing strengths to the sum of all rule firing strengths to compute the normalized firing strengths, and this is determined in each node using the following equation:

$$Q_{3,i} = \frac{w_i}{\sum w_i} = \frac{w_i}{w_1+w_2} = w_i \quad for \quad i = 1,2 \quad (13)$$

Layer 5 (consequent layer): Every node is an adaptive square node in this layer with the node function that makes the relation between inputs and outputs. It can be defined as the following equation:

$$Q_{4,1} = w_i.f_i = w_i.(p_ix + q_iy + r_i) \quad for \quad i = 1,2 \quad (14)$$

Layer 6 (inference): The output of this layer is the final result and is shown in the circle and labelled 'E'. It computes the sum of all incoming signals from the defuzzification layer to produce the overall output. It can be described as the following equation:

$$Q_{5,1} = \sum w_i.f_i = \frac{\sum w_i.f_i}{\sum w_i} = f_{out} \quad (15)$$

The structure of ANFIS is available in the Supplementary information.

2.4.2. Genetic algorithm (GA)

The genetic algorithm (GA) was first proposed by John Holland (Booker et al., 1989; Holland, 1992) who developed the conceptual and efficient structure in the design of GA. This algorithm was inspired by natural systems and was based on Darwin's theory (McCall, 2005). The GA is one of the most widely used evolutionary algorithms for optimization problems (Booker et al., 1989; Chen et al., 2017a; Delavar et al., 2004; Li and Yeh, 2005). Furthermore, selection, crossover, and mutation are fundamental components in GA as follows:

Selection operator: The fitness function is the essential part of the algorithm to test each chromosome in the population to see how it solved the goodness of the answer based on the problem. The GA converts each parameter value into a bit string by the sequence of 1s and 0s, and the strings link to each other to create the chromosomes (Jafari-Marandi and Smith, 2017). Each chromosome needs to be encoded, and the algorithm calculates the fitness value. Consequently, the population will be sorted according to individual fitness values (Jafari-Marandi and Smith, 2017). Every chromosome can be chosen, but the better fitness value will select a chromosome.

Crossover operator: Crossover is the pivotal operator of GA. This operator combines two entering chromosomes to produce a new chromosome (offspring). The idea behind crossover is that the new chromosome (offspring) may be the best characteristic that the entering chromosomes choose. The logic of crossover establishes the exploration of new solutions and exploitation of old solutions. The crossover operator can be implemented with different methods, including Ranking Selection, N-Point, Cycle, Order, Uniform, Tournament, and partially mapped (Saeidian et al., 2016). Since the use of a uniform method, such as the Crossover operator, is common among researchers (Vekaria and Clack, 1998), this method is utilized in the current study.

Mutation operator: Mutation is the most important operator in the GA. In this process a single chromosome enters and changes fast, without any reason, and alters randomly (Lebib et al., 2017). The result causes the local optimum to not be accepted as the best solution. To realize this goal, we only need to change some of the genes inside the chromosomes randomly.

The determination criterion decides on the last step of an evolutionary algorithm. The generation process is implemented until the specified termination criterion defines the end of the search procedure.

Examples of the selection, crossover, and mutation operators are in the Supplementary information.

2.4.3. Differential evolution (DE) algorithm

The differential evolution (DE) algorithm was presented by Storn and Price in the 1990s (Storn, 1999; Storn and Price, 1997). This algorithm has been widely recognized and utilized among researchers as an evolutionary algorithm that can optimize the solution to the problems with continuous space (Das et al., 2009). Similar to any other evolutionary algorithm, the DE algorithm first develops its initial population randomly. In fact, each individual in this population stands for a solution. Each individual is defined by a vector according to the following formula:

$$X_i^G = \left(x_{1,i}^G, x_{2,i}^G, x_{3,i}^G, \ldots, x_{D,i}^G\right) \quad (16)$$

where $i = \{0,1,2,\ldots,NP\}$, the number of the individuals in the population; D is the dimension of the problem or, in other words, the number of the parameters in the problem; $G = \{0,1,2,\ldots,G_{Max}\}$ is the generation time; and G_{Max} is the number of the last generation. After producing the initial population, by using mutation, crossover, and selection operators to generate better individuals, it is time to move to the next generation (Boussaïd et al., 2013). Its operators are as follows:

2.4.3.1. Mutation operation. The mutation operator produces a mutated vector (donor vector) $V_i^G = \{V_1^G, V_2^G, \ldots, V_D^G\}$ for the parent vector (target vector) X_i^G (Mukherjee et al., 2016; Zorlu, 2017). Many outstanding

relations have been introduced for the mutation operator, and the following ones can be referred to (Chen et al., 2017a; Li et al., 2014):

$$
\begin{aligned}
&DE/\ rand/1 : V_i^G = X_{r1}^G + F \cdot \left(X_{r2}^G - X_{r3}^G\right)\\
&DE/\ rand/2 : V_i^G = X_{r1}^G + F \cdot \left(X_{r2}^G - X_{r3}^G\right) + F \cdot \left(X_{r4}^G - X_{r5}^G\right).\\
&DE/best/1 : V_i^G = X_{best}^G + F \cdot \left(X_{r1}^G - X_{r2}^G\right)\\
&DE/best/2 : V_i^G = X_{best}^G + F \cdot \left(X_{r1}^G - X_{r2}^G\right) + F \cdot \left(X_{r3}^G - X_{r4}^G\right)\\
&DE/current\text{–}to\text{–}\ rand/1 : V_i^G = X_i^G + F \cdot \left(X_{r1}^G - X_i^G\right) + F \cdot \left(X_{r2}^G - X_{r3}^G\right)\\
&DE/current\text{–}to\text{–}\ rand/1 : V_i^G = X_i^G + F \cdot \left(X_{best}^G - X_i^G\right) + F \cdot \left(X_{r1}^G - X_{r2}^G\right)
\end{aligned}
\tag{17}
$$

where r_1, r_2, r_3, r_4 are integers randomly chosen from [0,NP] and comply with the $r_1 \neq r_2 \neq r_3 \neq r_4$ condition. F is a scale factor that determines the mutation scale; a random number chosen from [0,1]. X_{best}^G is an individual that enjoys the best fitness value in G, the generation population.

2.4.3.2. Crossover operation. The crossover operator uses a donor vector V_{ji}^G and target vector X_{ji}^G to produce a trial vector $U_{j,i}^G = \{u_{1,i}^G, u_{2,i}^G, \ldots, u_{D,i}^G\}$, which is described as

$$
U_{ji}^G = \begin{cases} V_{ji}^G & if\ \ rand\,[0,1] \leq CR\ \ or\ \ j = j_{rand} \\ X_{ji}^G & otherwise \end{cases}
\tag{18}
$$

where i∈{1,2,…,NP}, j∈{1,2,…,D}, j_{rand} are the random numbers in [1,D] and CR is the crossover rate, uniformly distributed random in [0,1].

2.4.3.3. Selection operation. As we compare the fitness value of trial vector U_i^G with target vector X_i^G, the best choice among them for the next generation is determined:

$$
X_i^{G+1} = \begin{cases} U_i^G & if\ f\left(U_i^G\right) \leq f\left(X_i^G\right) \\ X_i^G & \text{otherwise} \end{cases}
\tag{19}
$$

The flowchart of GA and DE is given in the Supplementary information.

2.5. Model evaluation using ROC method

The performance of the developed hybrid model was assessed using a standard technique namely, the Receiver Operating Characteristic (ROC), which has often been used in geo-hazard modelling studies (Chen et al., 2017c; Chen et al., 2017f; Chen et al., 2017g; Tien Bui et al., 2016b; Tien Bui et al., 2017). The ROC curve is based on the sensitivity (x-axis) and 100-specificity (y-axis) (Chapi et al., 2017). According to the definition, the sensitivity is the number of flood pixels classified as flood, and the specificity is the number of non-flood pixels that represent in reality non-flood. Quantitatively, the performance of new hybrid models was evaluated using the area under the ROC curve (AUC) that estimates the occurrence or non-occurrence of an event (Chen et al., 2017h; Yesilnacar and Topal, 2005). An AUC equal to 0.5 indicates significant inaccuracy of the model, whereas a model with ideal accuracy will have an AUC equal to 1 (Chen et al., 2017d). Thus, the higher the value of the AUC is, the better the performance of a model (Fawcett, 2006). The AUC is calculated by Eq. (20):

$$
\text{AUROC} = \frac{\dot{a}\text{TP} + \dot{a}\text{TN}}{\text{P} + \text{N}}
\tag{20}
$$

where TP and TN are the percentage of positive and negative instances that were correctly classified, P is the total number of floods and N is the total number of non-floods.

Table 1
Spatial relationship between floods and influencing factors by SWARA model.

Conditioning factors	Classes	No. of pixels	No. of flood	SWARA weight
Slope angle (°)	0–5	119,931	48	0.334
	5–10	181,016	62	0.257
	10–15	133,839	19	0.171
	15–30	227,219	5	0.143
	30–71.375	69,445	0	0.095
Aspect	Flat	234	0	0.008
	North	83,177	18	0.146
	Northeast	78,846	12	0.105
	East	86,019	21	0.161
	Southeast	99,478	19	0.127
	South	99,929	8	0.050
	Southwest	97,587	14	0.100
	West	95,554	19	0.133
	Northwest	90,626	23	0.169
Altitude (m)	<100	225,425	88	0.567
	100–200	246,261	45	0.354
	200–300	103,807	1	0.059
	300–400	57,942	0	0.010
	400–1347	98,015	0	0.010
Curvature	(−16.88)–(−1.148)	143,240	25	0.263
	(−1.148)–(−0.392)	136,121	27	0.219
	(−0.392)–(−0.237)	152,378	35	0.209
	(−0.237)–1.118	157,303	32	0.190
	1.118–15.222	142,408	15	0.119
STI	0–5	320,303	99	0.562
	5–10	151,163	17	0.208
	10–30	191,735	17	0.173
	30–50	40,618	1	0.029
	50–1458.205	27,631	0	0.028
Rainfall (mm)	1509.073–1700	30,164	3	0.257
	1700–1800	251,241	65	0.095
	1800–1900	203,199	30	0.171
	1900–2000	169,341	30	0.143
	>2000	77,432	6	0.334
SPI	0–50	570,286	117	0.367
	50–100	74,754	13	0.306
	100–150	28,373	4	0.245
	150–500	42,514	0	0.041
	500–49,279.836	15,522	0	0.041
TWI	2.365–5	185,558	5	0.038
	5–7	401,699	83	0.230
	7–9	109,997	34	0.345
	9–15	33,961	12	0.380
	15–29.770	235	0	0.006
Distance to rivers (m)	0–100	108,478	64	0.508
	100–200	95,903	20	0.175
	200–300	91,654	17	0.146
	300–400	78,038	12	0.122
	>400	357,377	21	0.049
Lithology	A	6372	3	0.177
	B	114,195	25	0.083
	C	149,392	42	0.109
	D	59,869	1	0.005
	E	3662	3	0.318
	F	257,766	20	0.030
	G	46,313	11	0.091
	H	27,518	3	0.041
	I	66,363	26	0.147
Soil type	ATc	124,487	50	0.360
	ACu	60,717	0	0.021
	ALh	6977	0	0.021
	RGd	14,834	7	0.468
	ACh	524,435	77	0.129
Land use	Barren land	5836	0	0.032
	Grass land	216,141	0	0.032
	Farm land	72,844	0	0.032
	Forest land	311,044	99	0.272
	Water body	20,277	11	0.436
	Residential area	105,308	24	0.195
NDVI	(−0.4712)–(−0.1233)	39,824	21	0.420
	(−0.1233)–(−0.0024)	135,421	55	0.323
	(−0.0024)–(0.1024)	178,899	48	0.215
	0.1024–0.2023	215,686	9	0.036
	0.2023–0.4725	161,620	1	0.006

3. Results and validation

3.1. Correlation between floods and conditioning factors using the SWARA model

Table 1 shows the correlation between floods and conditioning factors using the SWARA model. The results show that in the case of slope angle, the SWARA values are the highest for the class of 0°–5° (0.334), indicating that this class has the highest probability of flood occurrence. The results show that the highest SWARA values are calculated in the Northwest-facing (0.169) and east-facing (0.161) areas, whereas in the case of elevation, the SWARA values decrease as the altitude increases (the highest SWARA value appears in the class <100 m: 0.567). In the case of curvature, the highest SWARA value is in the class −16.88 to −1.148 (0.263). In the case of the STI, the highest SWARA value is in the class 0–5 (0.562). In the case of rainfall, the highest SWARA value is in the class >2000 (0.334). In the case of the SPI, the highest SWARA value is in the class 0–50 (0.367). In

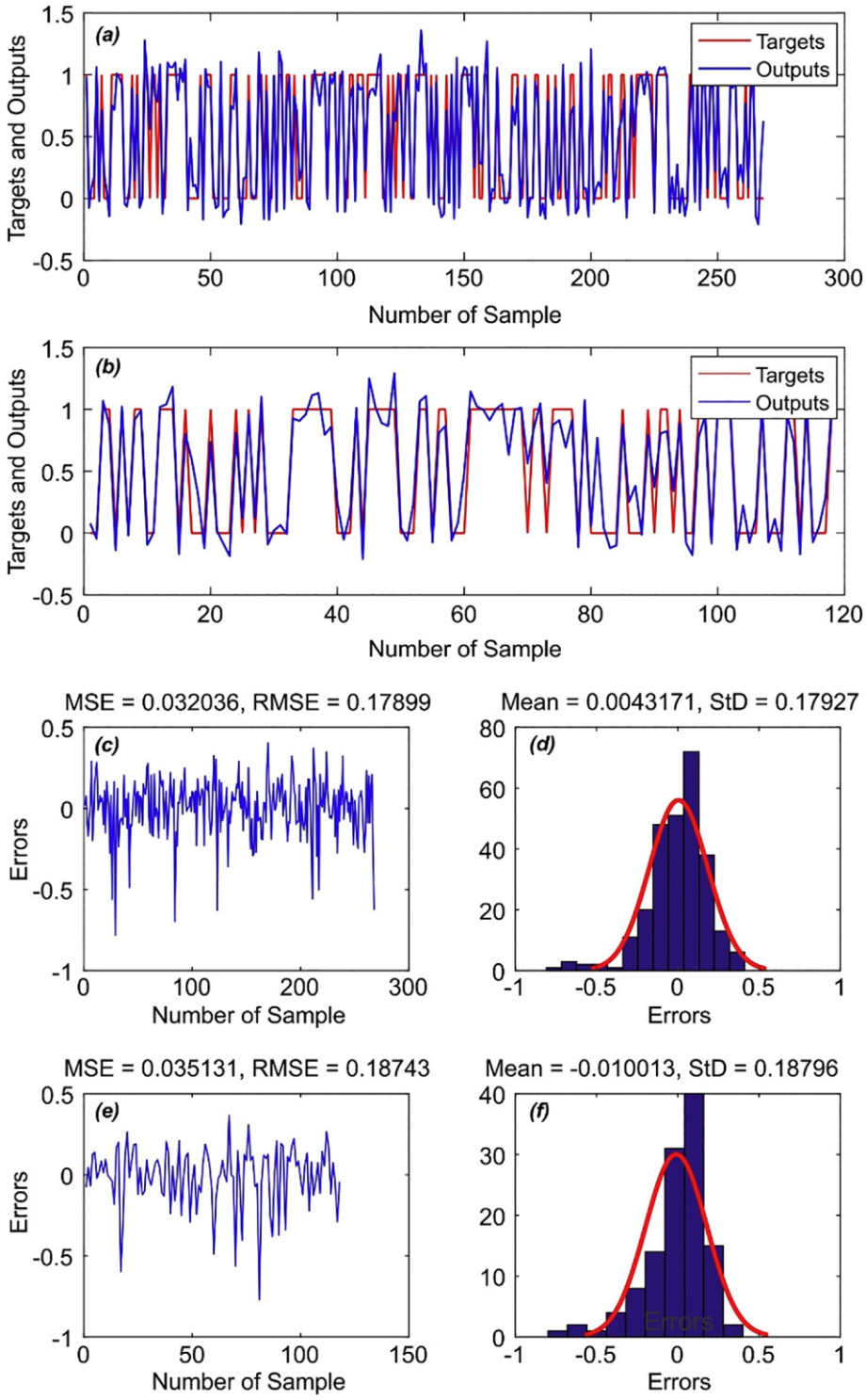

Fig. 5. ANFIS-DE model: a) target and output ANFIS-DE value of train data samples c) MSE and RMSE value of train data samples d) frequency errors of train data samples; b) target and output ANFIS-DE value of testing data samples e) MSE and RMSE value of testing data samples f) frequency errors of testing data samples.

the case of the TWI, the 9–15 class has the highest SWARA value of 0.380. For the distance to rivers, the class of 0–100 m showed the highest SWARA value of 0.508. The lithology in class E resulted in the highest SWARA value (0.318), whereas for soil type, it was the class of RGd (0.468). In the case of land use, the highest SWARA value was obviously in the classes of water bodies (0.436) and forest land (0.272), followed by residential areas (0.195). In the case of NDVI, the highest SWARA value was found in the class of (−0.4712)–(−0.1233).

3.2. Application of ANFIS ensemble models in flood susceptibility modelling

In the present study, a MATLAB code was developed to build the hybrid ANFIS-GA and ANFIS-DE models. Data were initially fed into these hybrid models to train them and assess their potential. The total number of flood events is 195. Also, number of NON-flood event is 195. As already mentioned, the collected data were divided randomly in a 70/30 ratio between training and validation data, respectively. The procedure is such that the gained weights from the SWARA method for each conditioning factor was fed as the input, and the values 0/1 for flood/non-flood were fed to the output. Figs. 4–5 illustrate the training method that aims to define the relationship between input/output by training the hybrid models ANFIS-GA and ANFIS-DE. To determine the accuracy of the validation, the RMSE statistical parameter was used:

$$\mathrm{RSME} = \sqrt{{}^{1}/_{n} \times \sum (TAG_i - OPT_i)^2} \quad (21)$$

where n is total samples in the training dataset or the test data set; TAG_i is the target values of the training dataset or the test data set; and OPT_i is output values from the hybrid models.

Figs. 4–5(c) show that the values of RMSE for ANFIS-GA and ANFIS-DE are 0.165 and 0.178, respectively, for the training phase. This finding shows that ANFIS-GA performed better than ANFIS-DE in the training phase. However, for determining the best model in optimization, the RMSE of the training phase is not sufficient and the RMSE of the test needs to be evaluated. According to the results, the RMSE of the ANFIS-GA and ANFIS-DE hybrid models was 0.182 and 0.187, respectively, which shows that the ANFIS-GA had again a relatively better performance compared to the ANFIS-DE, as shown in Figs. 4–5(e).

In addition to accuracy, computation time is also an important factor. The performance of both models was compared for 1000 iterations and the results were 300 s for ANFIS-GA and 95 s for ANFIS-DE, showing that the latter is much faster. The processing time of two hybrid models is available in the Supplementary material.

3.3. Flood susceptibility mapping using the ANFIS ensemble model

In the present study, the ANFIS ensemble model was developed using training data and SWARA values standardized between 0 and 1. The ANFIS-GA and ANFIS-DE models generated flood susceptibility maps for the Hengfeng area. The calculated flood susceptibility index (FSI) values for each pixel (pixel-by-pixel) were calculated in the GIS environment in order to design the final flood susceptibility maps. The flood susceptibility index (FSI) indicates the flood probability in a specific area based on previous observations. In other words, according to the type of defined model, the susceptibility is estimated for the whole region and is classified into five groups of very low, low, medium, high and very high. For comparison, Fig. 6 displays two flood susceptibility maps produced from the ANFIS-GA and ANFIS-DE models. The five flood susceptibility classes for both ANFIS-GA and ANFIS-DE models are very low, low, moderate, high, and very high.

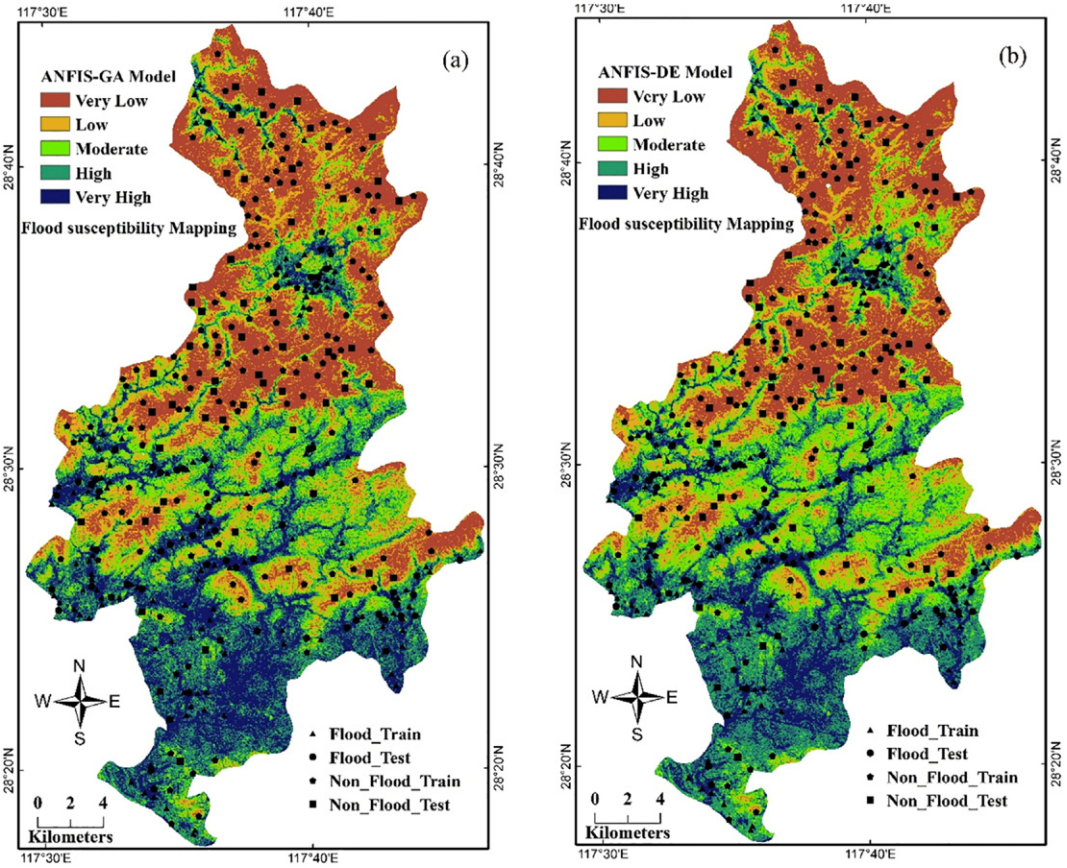

Fig. 6. a) Flood susceptibility map by ANFIS-GA model, b) ANFIS-DE model.

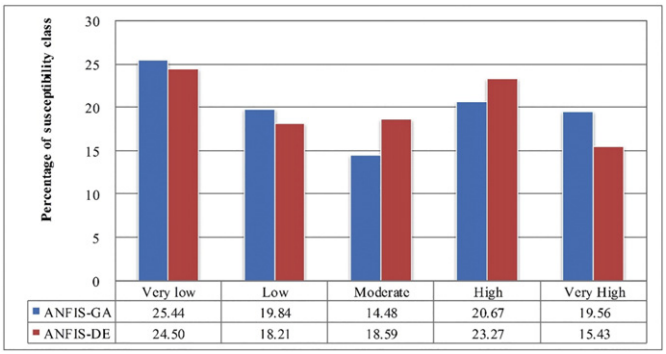

Fig. 7. Percentages of different flood susceptibility classes.

Fig. 7 displays the area percentages of each class for both. It appears that according to the ANFIS-GA model, the very low class has the largest area (25.44%), followed by the high (20.67%), and low (19.84%) classes. In the ANFIS-DE model, the percentages are 24.50%, 18.21%, 18.59%, 23.27% and 15.43% for the very low, low, moderate, high, and very high classes, respectively.

3.4. Validation of the flood susceptibility maps

The receiver operating characteristic curve (ROC) that was used to train the dataset for both flood susceptibility maps is shown in Fig. 8a. The results show that the ANFIS-DE model achieved the highest AUC value of 0.8523, and the ANFIS-GA had an AUC value of 0.8488. The ROC plots using the testing dataset for the two flood susceptibility maps are shown in Fig. 8b. The results show that the ANFIS-GA model exhibited the highest AUC value of 0.8743, whereas the ANFIS-DE had a lower AUC value equal to 0.8686. These results are in line with the results of the MSE values in the testing phase. Therefore, according to the results, we can conclude that both models show a reasonable ROC, with the ANFIS-DE model achieving a better performance in flood susceptibility projection compared to the ANFIS-GA model.

4. Discussion

Flooding is a very complex process that is controlled by many environmental factors. For instance, climatic parameters strongly influence flood events. However, climate change determines a variable environment, where extreme weather events occur more rapidly inducing natural hazards such as floods To the best of our knowledge, extreme events in the Hengfeng area have not been sufficiently studied to date. The present study aims to cover this knowledge gap by using a spatial approach that includes artificial intelligence, resulting in an "ensemble" method. Similar studies have focused on the large-scale assessment of flood susceptibility in Europe, Asia, and America. However, there is still uncertainty regarding the impact that climate change has on flood events. Understanding as accurately as possible the seasonality of the climatic factors, especially under dynamic climate change, is important for the assessment of flood occurrence. Human activity is another important factor influencing flood occurrence and development. Land use and river courses may change due to population growth, industrial development, and urbanization, so flood susceptibility might be affected. In the current literature, one can find several approaches for establishing the relationship between floods and their influencing factors, such as the probability certainty factor, statistical index, gain ratio, chi-square, and relief significance. However, a global debate is still in progress regarding the most suitable model for flood susceptibility assessment. In the future, for flood susceptibility mapping in a single flood event, we may use extreme rainfall or maximum three-day rainfall as an induced factor coupled with the results of a flood simulation model with depth, duration and velocity (Wang et al., 2015). In fact,

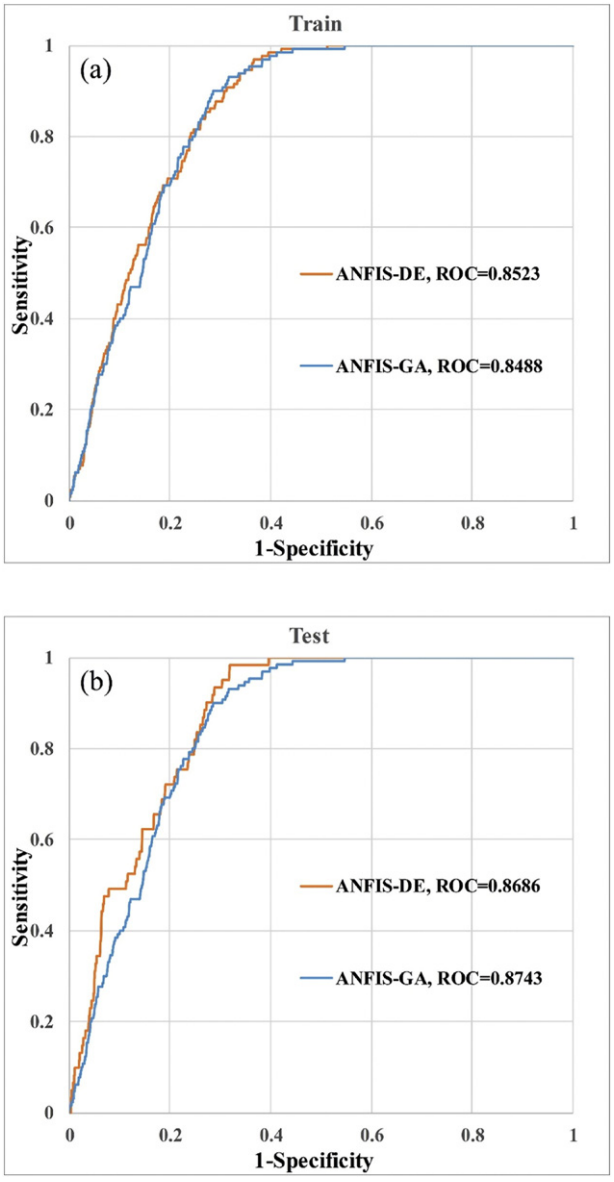

Fig. 8. ROC curves for the ANFIS-GA and ANFIS-DE model.

such models are influenced by the local hydrological, geological, hydrogeological and morphological conditions, and researchers tend to adapt and calibrate them to obtain the optimal solution in a specific study area (Shafapour Tehrany et al., 2017). Tehrany et al. (2015a, 2015b, 2015c) compared the support vector machine model with different kernel types for flood susceptibility mapping in Kuala Terengganu, Malaysia. Their results stated that the support vector machine with a radial basis kernel showed the best performance (Tehrany et al., 2015c).

Recently, several ensemble methods have been developed, including an ensemble of bivariate and multivariate statistical models (Tehrany et al., 2013b), weights-of-evidence and support vector machine (Tehrany et al., 2014b), and the support vector machine and frequency ratio (Tehrany et al., 2015b). The advantage of such methods for flood susceptibility assessment is that they facilitate visualization while achieving more accurate projections than single machine learning models (Chen et al., 2017b). Additionally, ensemble models do not have the weaknesses of bivariate statistical analysis and machine learning methods (Tehrany et al., 2013b). This has led to their increased popularity among researchers in flood-related studies (Chen et al., 2017b). In the present study, the flood susceptibility maps are consistent and in

accordance with the historical flood events. The wackiness of such methods is the incapability to estimate flood depth, velocity and duration. In future studies, the flood susceptibility assessment results should be compared with flood simulation models to overcome the aforementioned drawback.

5. Conclusions

Flood susceptibility assessment is of the utmost importance to prevent human casualties and socio-economic losses. Flood management should be a priority, particularly in emerging economies with high developing targets, such as China. In this study, an innovative method for flood susceptibility mapping was developed by coupling an adaptive neuro-fuzzy inference system (ANFIS) with a genetic algorithm and differential evolution. Hengfeng County was selected for the application of these methods due to the affluence of the necessary data and the occurrence of 195 flood events. The developed model involves thirteen flood conditioning factors, and all data were elaborated in a GIS environment. The SWARA model was used to determine the relationship between the floods and influencing factors. Subsequently, two data mining techniques were combined with the ANFIS model, including ANFIS-Genetic Algorithm (ANFIS-GA) and ANFIS-Differential Evolution (ANFIS-DE) for the flood spatial modelling and its zonation. The flood susceptibility maps were evaluated by the ROC curve, and the performance of all models was tested using the RMSE and MSE method. The area under the curve (AUC) of all of the models was >0.80. Moreover, the highest AUC value was found for the ANFIS-DE model (0.8523), followed by ANFIS-GA (0.8490). In addition to accuracy, computation time is an important factor. The performance of both models was compared for 1000 iterations, and the results were 300 s for ANFIS-GA and 95 s for ANFIS-DE, which shows that the latter is much faster. The hybrid model of ANFIS-DE is selected as the most suitable model in the flood susceptibility mapping. In general, the proposed ensemble data mining techniques can be used for land use planning and for managing flood susceptibility and hazards in both the study area and other areas.

Acknowledgements

We express our great thanks to Wei Ouyang, Associate Editor of the journal Science of the Total Environment and all reviewers, with their comments and suggestions, which improved the quality of our paper. National Natural Science Foundation of China (Project No.: 41431177, 41601413), Natural Science Research Program of Jiangsu (Project No.: BK20150975), Natural Science Research Program of Jiangsu (Project No.: 14KJA170001), National Basic Research Program of China (Project No.: 2015CB954102), and CAS-VPST Silk Road Science Fund 2018 (Grant No. GJHZ1855). Support to A-Xing Zhu through the Vilas Associate Award, the Hammel Faculty Fellow Award, the Manasse Chair Professorship from the University of Wisconsin-Madison, and the "One-Thousand Talents" Program of China is greatly appreciated. We thank the Baidu Company (www.baidu.com) for providing the flood event photo.

Appendix A. Supplementary data

Supplementary data to this article can be found online at https://doi.org/10.1016/j.scitotenv.2017.10.114.

References

Aalto, R., Maurice-Bourgoin, L., Dunne, T., Montgomery, D.R., Nittrouer, C.A., Guyot, J.-L., 2003. Episodic sediment accumulation on Amazonian flood plains influenced by El Nino/Southern Oscillation. Nature 425, 493–497.

Adam, T.N., David, M.C., 2011. Relationships between Arctic shrub dynamics and topographically derived hydrologic characteristics. Environ. Res. Lett. 6, 045506.

Aissia, M.A.B., Chebana, F., Ouarda, T.B.M.J., Roy, L., Desrochers, G., Chartier, I., et al., 2012. Multivariate analysis of flood characteristics in a climate change context of the watershed of the Baskatong reservoir, province of Québec, Canada. Hydrol. Process. 26, 130–142.

Alimardani, M., Hashemkhani Zolfani, S., Aghdaie, M.H., Tamošaitienė, J., 2013. A novel hybrid SWARA and VIKOR methodology for supplier selection in an agile environment. Technol. Econ. Dev. Econ. 19, 533–548.

Antonelli, C., Eyrolle, F., Rolland, B., Provansal, M., Sabatier, F., 2008. Suspended sediment and 137Cs fluxes during the exceptional December 2003 flood in the Rhone River, southeast France. Geomorphology 95, 350–360.

Arnell, N.W., Gosling, S.N., 2016. The impacts of climate change on river flood risk at the global scale. Clim. Chang. 134, 387–401.

Asadi, H.H., Porwal, A., Fatehi, M., Kianpouryan, S., Lu, Y.-J., 2015. Exploration feature selection applied to hybrid data integration modeling: targeting copper-gold potential in central Iran. Ore Geol. Rev. 71, 819–838.

Bahremand, A., De Smedt, F., Corluy, J., Liu, Y.B., Poorova, J., Velcicka, L., et al., 2007. WetSpa model application for assessing reforestation impacts on floods in Margecany–Hornad watershed, Slovakia. Water Resour. Manag. 21, 1373–1391.

Barker, D.M., Lawler, D.M., Knight, D.W., Morris, D.G., Davies, H.N., Stewart, E.J., 2009. Longitudinal distributions of river flood power: the combined automated flood, elevation and stream power (CAFES) methodology. Earth Surf. Process. Landf. 34, 280–290.

Beckers, A., Dewals, B., Erpicum, S., Dujardin, S., Detrembleur, S., Teller, J., et al., 2013. Contribution of land use changes to future flood damage along the river Meuse in the Walloon region. Nat. Hazards Earth Syst. Sci. 13, 2301–2318.

Benito, G., Rico, M., Sánchez-Moya, Y., Sopeña, A., Thorndycraft, V.R., Barriendos, M., 2010. The impact of late Holocene climatic variability and land use change on the flood hydrology of the Guadalentín River, southeast Spain. Glob. Planet. Chang. 70, 53–63.

Billi, P., 2011. Flash flood sediment transport in a steep sand-bed ephemeral stream. International Journal of Sediment Research 26, 193–209.

Booker, L.B., Goldberg, D.E., Holland, J.H., 1989. Classifier systems and genetic algorithms. Artif. Intell. 40, 235–282.

Bouilloud, L., Delrieu, G., Boudevillain, B., Kirstetter, P.-E., 2010. Radar rainfall estimation in the context of post-event analysis of flash-flood events. J. Hydrol. 394, 17–27.

Boussaïd, I., Lepagnot, J., Siarry, P.A., 2013. Survey on optimization metaheuristics. Inf. Sci. 237, 82–117.

Cardenas, M.B., Wilson, J.L., Zlotnik, V.A., 2004. Impact of heterogeneity, bed forms, and stream curvature on subchannel hyporheic exchange. Water Resour. Res. 40 (n/a-n/a).

Çelik, H.E., Coskun, G., Cigizoglu, H.K., Ağıralioğlu, N., Aydın, A., Esin, A.İ., 2012. The analysis of 2004 flood on Kozdere Stream in Istanbul. Nat. Hazards 63, 461–477.

Celikyilmaz, A., Turksen, I.B., 2009. Modeling uncertainty with fuzzy logic. Stud. Fuzziness Soft Comput. 240, 149–215.

Chapi, K., Singh, V.P., Shirzadi, A., Shahabi, H., Bui, D.T., Pham, B.T., et al., 2017. A novel hybrid artificial intelligence approach for flood susceptibility assessment. Environ. Model. Softw. 95, 229–245.

Charlton, R., Fealy, R., Moore, S., Sweeney, J., Murphy, C., 2006. Assessing the impact of climate change on water supply and flood hazard in Ireland using statistical downscaling and hydrological modelling techniques. Clim. Chang. 74, 475–491.

Chau, K., Wu, C., Li, Y., 2005. Comparison of several flood forecasting models in Yangtze River. J. Hydrol. Eng. 10, 485–491.

Chen, C.-Y., Yu, F.-C., 2011. Morphometric analysis of debris flows and their source areas using GIS. Geomorphology 129, 387–397.

Chen, H., Ito, Y., Sawamukai, M., Tokunaga, T., 2015. Flood hazard assessment in the Kujukuri Plain of Chiba Prefecture, Japan, based on GIS and multicriteria decision analysis. Nat. Hazards 78, 105–120.

Chen, W., Panahi, M., Pourghasemi, H.R., 2017a. Performance evaluation of GIS-based new ensemble data mining techniques of adaptive neuro-fuzzy inference system (ANFIS) with genetic algorithm (GA), differential evolution (DE), and particle swarm optimization (PSO) for landslide spatial modelling. Catena 157, 310–324.

Chen, W., Pourghasemi, H.R., Kornejady, A., Zhang, N., 2017b. Landslide spatial modeling: introducing new ensembles of ANN, MaxEnt, and SVM machine learning techniques. Geoderma 305, 314–327.

Chen, W., Pourghasemi, H.R., Panahi, M., Kornejady, A., Wang, J., Xie, X., et al., 2017c. Spatial prediction of landslide susceptibility using an adaptive neuro-fuzzy inference system combined with frequency ratio, generalized additive model, and support vector machine techniques. Geomorphology 297, 69–85.

Chen, W., Pourghasemi, H.R., Zhao, Z.A., 2017d. GIS-based comparative study of Dempster-Shafer, logistic regression and artificial neural network models for landslide susceptibility mapping. Geocarto Int. 32, 367–385.

Chen, W., Xie, X., Peng, J., Wang, J., Duan, Z., Hong, H., 2017e. GIS-based landslide susceptibility modelling: a comparative assessment of kernel logistic regression, Naïve-Bayes tree, and alternating decision tree models. Geomatics Nat. Hazards Risk 1–24.

Chen, W., Xie, X., Wang, J., Pradhan, B., Hong, H., Tien Bui, D., et al., 2017f. A comparative study of logistic model tree, random forest, and classification and regression tree models for spatial prediction of landslide susceptibility. Catena 151, 147–160.

Chen, W., Pourghasemi, H.R., Naghibi, S.A., 2017g. A comparative study of landslide susceptibility maps produced using support vector machine with different kernel functions and entropy data mining models in China. Bull. Eng. Geol. Environ. 1–18.

Chen, W., Pourghasemi, H.R., Naghibi, S.A., 2017h. Prioritization of landslide conditioning factors and its spatial modeling in Shangnan County, China using GIS-based data mining algorithms. Bull. Eng. Geol. Environ. 1–19.

Das, S., Abraham, A., Chakraborty, U.K., Konar, A., 2009. Differential evolution using a neighborhood-based mutation operator. IEEE Trans. Evol. Comput. 13, 526–553.

Dehnavi, A., Aghdam, I.N., Pradhan, B., Morshed Varzandeh, M.H., 2015. A new hybrid model using step-wise weight assessment ratio analysis (SWARA) technique and adaptive neuro-fuzzy inference system (ANFIS) for regional landslide hazard assessment in Iran. Catena 135, 122–148.

Delavar, M., Samadzadegan, F., Pahlavani, P., 2004. A GIS-assisted optimal urban route finding approach based on genetic algorithms. Int. Arch. Photogramm. Remote. Sens. Spat. Inf. Sci. 35, 305–308.

Dobler, C., Bürger, G., Stötter, J., 2012. Assessment of climate change impacts on flood hazard potential in the Alpine Lech watershed. J. Hydrol. 460, 29–39.
Dottori, F., Salamon, P., Bianchi, A., Alfieri, L., Hirpa, F.A., Feyen, L., 2016. Development and evaluation of a framework for global flood hazard mapping. Adv. Water Resour. 94, 87–102.
Du, J., Qian, L., Rui, H., Zuo, T., Zheng, D., Xu, Y., et al., 2012. Assessing the effects of urbanization on annual runoff and flood events using an integrated hydrological modeling system for Qinhuai River basin, China. J. Hydrol. 464, 127–139.
Emerton, R., Cloke, H.L., Stephens, E.M., Zsoter, E., Woolnough, S.J., Pappenberger, F., 2017. Complex picture for likelihood of ENSO-driven flood hazard. Nat. Commun. 8, 14796.
Ettinger, S., Mounaud, L., Magill, C., Yao-Lafourcade, A.-F., Thouret, J.-C., Manville, V., et al., 2016. Building vulnerability to hydro-geomorphic hazards: estimating damage probability from qualitative vulnerability assessment using logistic regression. J. Hydrol. 541, 563–581.
Fawcett, T., 2006. An introduction to ROC analysis. Pattern Recogn. Lett. 27, 861–874.
Fernández, D.S., Lutz, M.A., 2010. Urban flood hazard zoning in Tucumán Province, Argentina, using GIS and multicriteria decision analysis. Eng. Geol. 111, 90–98.
Flügel, W.-A., 1995. Delineating hydrological response units by geographical information system analyses for regional hydrological modelling using PRMS/MMS in the drainage basin of the River Bröl, Germany. Hydrol. Process. 9, 423–436.
Fuller, I.C., 2008. Geomorphic impacts of a 100-year flood: Kiwitea Stream, Manawatu catchment, New Zealand. Geomorphology 98, 84–95.
García-Ruiz, J.M., Regüés, D., Alvera, B., Lana-Renault, N., Serrano-Muela, P., Nadal-Romero, E., et al., 2008. Flood generation and sediment transport in experimental catchments affected by land use changes in the central Pyrenees. J. Hydrol. 356, 245–260.
Goel, N.K., Kurothe, R.S., Mathur, B.S., Vogel, R.M., 2000. A derived flood frequency distribution for correlated rainfall intensity and duration. J. Hydrol. 228, 56–67.
Gutiérrez-Jurado, H.A., Vivoni, E.R., Istanbulluoglu, E., Bras, R.L., 2007. Ecohydrological response to a geomorphically significant flood event in a semiarid catchment with contrasting ecosystems. Geophys. Res. Lett. 34 (n/a-n/a).
Hagen, E., Shroder, J.F., XX, Lu, Teufert, J.F., 2010. Reverse engineered flood hazard mapping in Afghanistan: a parsimonious flood map model for developing countries. Quat. Int. 226, 82–91.
Hashemkhani Zolfani, S., Bahrami, M., 2014. Investment prioritizing in high tech industries based on SWARA-COPRAS approach. Technol. Econ. Dev. Econ. 20, 534–553.
He, B., Y-G, Xu, Huang, X.-L., Luo, Z.-Y., Shi, Y.-R., Yang, Q.-J., et al., 2007. Age and duration of the Emeishan flood volcanism, SW China: geochemistry and SHRIMP zircon U–Pb dating of silicic ignimbrites, post-volcanic Xuanwei Formation and clay tuff at the Chaotian section. Earth Planet. Sci. Lett. 255, 306–323.
Ho, L.T.K., Umitsu, M., 2011. Micro-landform classification and flood hazard assessment of the Thu Bon alluvial plain, central Vietnam via an integrated method utilizing remotely sensed data. Appl. Geogr. 31, 1082–1093.
Holland, J.H., 1992. Adaptation in Natural and Artificial Systems: An Introductory Analysis With Applications to Biology, Control, and Artificial Intelligence. MIT Press.
Horritt, M.S., 2000. Calibration of a two-dimensional finite element flood flow model using satellite radar imagery. Water Resour. Res. 36, 3279–3291.
Huang, S., Li, J., Xu, M., 2012. Water surface variations monitoring and flood hazard analysis in Dongting Lake area using long-term Terra/MODIS data time series. Nat. Hazards 62, 93–100.
Hudson, P.F., Kesel, R.H., 2000. Channel migration and meander-bend curvature in the lower Mississippi River prior to major human modification. Geology 28, 531–534.
Jafari-Marandi, R., Smith, B.K., 2017. Fluid genetic algorithm (FGA). J. Comput. Des. Eng. 4, 158–167.
Jahed Armaghani, D., Hajihassani, M., Monjezi, M., Mohamad, E.T., Marto, A., Moghaddam, M.R., 2015. Application of two intelligent systems in predicting environmental impacts of quarry blasting. Arab. J. Geosci. 8, 9647–9665.
Jang, J.-S., 1993. ANFIS: adaptive-network-based fuzzy inference system. IEEE Trans. Syst. Man Cybern. 23, 665–685.
Johnson, L.E., 2000. Assessment of flash flood warning procedures. J. Geophys. Res. Atmos. 105, 2299–2313.
Kay, A.L., Jones, R.G., Reynard, N.S., 2006. RCM rainfall for UK flood frequency estimation. II. Climate change results. J. Hydrol. 318, 163–172.
Kazakis, N., Kougias, I., Patsialis, T., 2015. Assessment of flood hazard areas at a regional scale using an index-based approach and Analytical Hierarchy Process: application in Rhodope–Evros region, Greece. Sci. Total Environ. 538, 555–563.
Keršuliene, V., Zavadskas, E.K., Turskis, Z., 2010. Selection of rational dispute resolution method by applying new step-wise weight assessment ratio analysis (Swara). J. Bus. Econ. Manag. 11, 243–258.
Kia, M.B., Pirasteh, S., Pradhan, B., Mahmud, A.R., Sulaiman, W.N.A., Moradi, A., 2012. An artificial neural network model for flood simulation using GIS: Johor River Basin, Malaysia. Environ. Earth Sci. 67, 251–264.
Knighton, A.D., 1999. Downstream variation in stream power. Geomorphology 29, 293–306.
Kumar, R., Acharya, P., 2016. Flood hazard and risk assessment of 2014 floods in Kashmir Valley: a space-based multisensor approach. Nat. Hazards 84, 437–464.
Lebib, F.Z., Mellah, H., Drias, H., 2017. Enhancing information source selection using a genetic algorithm and social tagging. Int. J. Inf. Manag.
Li, X., Yeh, A.G.O., 2005. Integration of genetic algorithms and GIS for optimal location search. Int. J. Geogr. Inf. Sci. 19, 581–601.
Li, K., Wu, S., Dai, E., Xu, Z., 2012. Flood loss analysis and quantitative risk assessment in China. Nat. Hazards 63, 737–760.
Li, K., Zhang, Q., Kwong, S., Li, M., Wang, R., 2014. Stable matching-based selection in evolutionary multiobjective optimization. IEEE Trans. Evol. Comput. 18, 909–923.
Liu, K., Li, Z., Yao, C., Chen, J., Zhang, K., Saifullah, M., 2016. Coupling the k-nearest neighbor procedure with the Kalman filter for real-time updating of the hydraulic model in flood forecasting. Int. J. Sediment Res. 31, 149–158.
López-Tarazón, J.A., Batalla, R.J., Vericat, D., Balasch, J.C., 2010. Rainfall, runoff and sediment transport relations in a mesoscale mountainous catchment: the River Isábena (Ebro basin). Catena 82, 23–34.
Marchetti, Z.Y., Minotti, P.G., Ramonell, C.G., Schivo, F., Kandus, P., 2016. NDVI patterns as indicator of morphodynamic activity in the middle Paraná River floodplain. Geomorphology 253, 146–158.
Mathur, N., Glesk, I., Buis, A., 2016. Comparison of adaptive neuro-fuzzy inference system (ANFIS) and Gaussian processes for machine learning (GPML) algorithms for the prediction of skin temperature in lower limb prostheses. Med. Eng. Phys. 38, 1083–1089.
McCall, J., 2005. Genetic algorithms for modelling and optimisation. J. Comput. Appl. Math. 184, 205–222.
Moore, I.D., Grayson, R.B., Ladson, A.R., 1991. Digital terrain modelling: a review of hydrological, geomorphological, and biological applications. Hydrol. Process. 5, 3–30.
Mukerji, A., Chatterjee, C., Raghuwanshi, N.S., 2009. Flood forecasting using ANN, neuro-fuzzy, and neuro-GA models. J. Hydrol. Eng. 14, 647–652.
Mukherjee, R., Debchoudhury, S., Das, S., 2016. Modified differential evolution with locality induced genetic operators for dynamic optimization. Eur. J. Oper. Res. 253, 337–355.
Naik, P.K., Jay, D.A., 2011. Distinguishing human and climate influences on the Columbia River: changes in mean flow and sediment transport. J. Hydrol. 404, 259–277.
Najah, A., El-Shafie, A., Karim, O.A., El-Shafie, A.H., 2014. Performance of ANFIS versus MLP-NN dissolved oxygen prediction models in water quality monitoring. Environ. Sci. Pollut. Res. 21, 1658–1670.
Nandi, A., Mandal, A., Wilson, M., Smith, D., 2016. Flood hazard mapping in Jamaica using principal component analysis and logistic regression. Environ. Earth Sci. 75, 465.
Nedkov, S., Burkhard, B., 2012. Flood regulating ecosystem services—mapping supply and demand, in the Etropole municipality, Bulgaria. Ecol. Indic. 21, 67–79.
Norbiato, D., Borga, M., Degli Esposti, S., Gaume, E., Anquetin, S., 2008. Flash flood warning based on rainfall thresholds and soil moisture conditions: an assessment for gauged and ungauged basins. J. Hydrol. 362, 274–290.
Nunes Correia, F., Castro Rego, F., Da Graça Saraiva, M., Ramos, I., 1998. Coupling GIS with hydrologic and hydraulic flood modelling. Water Resour. Manag. 12, 229–249.
Oeurng, C., Sauvage, S., Sánchez-Pérez, J.-M., 2011. Assessment of hydrology, sediment and particulate organic carbon yield in a large agricultural catchment using the SWAT model. J. Hydrol. 401, 145–153.
Oh, H.-J., Pradhan, B., 2011. Application of a neuro-fuzzy model to landslide-susceptibility mapping for shallow landslides in a tropical hilly area. Comput. Geosci. 37, 1264–1276.
Onat, N., Ersoz, S., 2011. Analysis of wind climate and wind energy potential of regions in Turkey. Energy 36, 148–156.
Papaioannou, G., Vasiliades, L., Loukas, A., 2015. Multi-criteria analysis framework for potential flood prone areas mapping. Water Resour. Manag. 29, 399–418.
Phootrakornchai, W., Jiriwibhakorn, S., 2015. Online critical clearing time estimation using an adaptive neuro-fuzzy inference system (ANFIS). Int. J. Electr. Power Energy Syst. 73, 170–181.
Predick, K.I., Turner, M.G., 2008. Landscape configuration and flood frequency influence invasive shrubs in floodplain forests of the Wisconsin River (USA). J. Ecol. 96, 91–102.
Pulvirenti, L., Pierdicca, N., Chini, M., Guerriero, L., 2011. An algorithm for operational flood mapping from Synthetic Aperture Radar (SAR) data using fuzzy logic. Nat. Hazards Earth Syst. Sci. 11, 529–540.
Rahmati, O., Pourghasemi, H.R., Zeinivand, H., 2016. Flood susceptibility mapping using frequency ratio and weights-of-evidence models in the Golastan Province, Iran. Geocarto Int. 31, 42–70.
Rashid, H., 2011. Interpreting flood disasters and flood hazard perceptions from newspaper discourse: tale of two floods in the Red River valley, Manitoba, Canada. Appl. Geogr. 31, 35–45.
Reager, J.T., Thomas, B.F., Famiglietti, J.S., 2014. River basin flood potential inferred using GRACE gravity observations at several months lead time. Nat. Geosci. 7, 588–592.
Reneau, S.L., 2000. Stream incision and terrace development in Frijoles Canyon, Bandelier National Monument, New Mexico, and the influence of lithology and climate. Geomorphology 32, 171–193.
Rezakazemi, M., Dashti, A., Asghari, M., Shirazian, S., 2017. H2-selective mixed matrix membranes modeling using ANFIS, PSO-ANFIS, GA-ANFIS. Int. J. Hydrog. Energy 42, 15211–15225.
Robins, C.R., Buck, B.J., Williams, A.J., Morton, J.L., House, P.K., Howell, M.S., et al., 2009. Comparison of flood hazard assessments on desert piedmonts and playas: a case study in Ivanpah Valley, Nevada. Geomorphology 103, 520–532.
Rojas, R., Feyen, L., Bianchi, A., Dosio, A., 2012. Assessment of future flood hazard in Europe using a large ensemble of bias-corrected regional climate simulations. J. Geophys. Res. Atmos. 117 (n/a-n/a).
Rozalis, S., Morin, E., Yair, Y., Price, C., 2010. Flash flood prediction using an uncalibrated hydrological model and radar rainfall data in a Mediterranean watershed under changing hydrological conditions. J. Hydrol. 394, 245–255.
Saeidian, B., Mesgari, M.S., Ghodousi, M., 2016. Evaluation and comparison of Genetic Algorithm and Bees Algorithm for location–allocation of earthquake relief centers. Int. J. Disaster Risk Reduction 15, 94–107.
Sampson, C.C., Smith, A.M., Bates, P.D., Neal, J.C., Alfieri, L., Freer, J.E., 2015. A high-resolution global flood hazard model. Water Resour. Res. 51, 7358–7381.
Santangelo, N., Santo, A., Di Crescenzo, G., Foscari, G., Liuzza, V., Sciarrotta, S., et al., 2011. Flood susceptibility assessment in a highly urbanized alluvial fan: the case study of Sala Consilina (southern Italy). Nat. Hazards Earth Syst. Sci. 11, 2765–2780.
Segond, M.-L., Wheater, H.S., Onof, C., 2007. The significance of spatial rainfall representation for flood runoff estimation: a numerical evaluation based on the Lee catchment, UK. J. Hydrol. 347, 116–131.
Shafapour Tehrany, M., Shabani, F., Neamah Jebur, M., Hong, H., Chen, W., Xie, X., 2017. GIS-based spatial prediction of flood prone areas using standalone frequency ratio,

logistic regression, weight of evidence and their ensemble techniques. Geomatics Nat. Hazards Risk 1–24.
Slater, L.J., Singer, M.B., Kirchner, J.W., 2015. Hydrologic versus geomorphic drivers of trends in flood hazard. Geophys. Res. Lett. 42, 2014GL062482.
Soulsby, C., Tetzlaff, D., Hrachowitz, M., 2010. Spatial distribution of transit times in montane catchments: conceptualization tools for management. Hydrol. Process. 24, 3283–3288.
Stefanidis, S., Stathis, D., 2013. Assessment of flood hazard based on natural and anthropogenic factors using analytic hierarchy process (AHP). Nat. Hazards 68, 569–585.
Storn, R., 1999. System design by constraint adaptation and differential evolution. IEEE Trans. Evol. Comput. 3, 22–34.
Storn, R., Price, K., 1997. Differential evolution – a simple and efficient heuristic for global optimization over continuous spaces. J. Glob. Optim. 11, 341–359.
Suriya, S., Mudgal, B.V., 2012. Impact of urbanization on flooding: the Thirusoolam sub watershed – a case study. J. Hydrol. 412, 210–219.
Tehrany, M.S., Pradhan, B., Jebur, M.N., 2013a. Spatial prediction of flood susceptible areas using rule based decision tree (DT) and a novel ensemble bivariate and multivariate statistical models in GIS. J. Hydrol. 504, 69–79.
Tehrany, M.S., Pradhan, B., Jebur, M.N., 2013b. Spatial prediction of flood susceptible areas using rule based decision tree (DT) and a novel ensemble bivariate and multivariate statistical models in GIS. J. Hydrol. 504, 69–79.
Tehrany, M.S., Pradhan, B., Jebur, M.N., 2014a. Flood susceptibility mapping using a novel ensemble weights-of-evidence and support vector machine models in GIS. J. Hydrol. 512, 332–343.
Tehrany, M.S., Pradhan, B., Jebur, M.N., 2014b. Flood susceptibility mapping using a novel ensemble weights-of-evidence and support vector machine models in GIS. J. Hydrol. 512, 332–343.
Tehrany, M.S., Pradhan, B., Mansor, S., Ahmad, N., 2015a. Flood susceptibility assessment using GIS-based support vector machine model with different kernel types. Catena 125, 91–101.
Tehrany, M.S., Pradhan, B., Jebur, M.N., 2015b. Flood susceptibility analysis and its verification using a novel ensemble support vector machine and frequency ratio method. Stoch. Env. Res. Risk A. 29, 1149–1165.
Tehrany, M.S., Pradhan, B., Jebur, M.N., 2015c. Flood susceptibility analysis and its verification using a novel ensemble support vector machine and frequency ratio method. Stoch. Env. Res. Risk A. 29, 1149–1165.
Tien Bui, D., Pradhan, B., Nampak, H., Bui, Q.-T., Tran, Q.-A., Nguyen, Q.-P., 2016a. Hybrid artificial intelligence approach based on neural fuzzy inference model and metaheuristic optimization for flood susceptibility modeling in a high-frequency tropical cyclone area using GIS. J. Hydrol. 540, 317–330.
Tien Bui, D., Pradhan, B., Nampak, H., Bui, Q.T., Tran, Q.A., Nguyen, Q.P., 2016b. Hybrid artificial intelligence approach based on neural fuzzy inference model and metaheuristic optimization for flood susceptibility modeling in a high-frequency tropical cyclone area using GIS. J. Hydrol. 540, 317–330.
Tien Bui, D., Tuan, T.A., Hoang, N.-D., Thanh, N.Q., Nguyen, D.B., Van Liem, N., et al., 2017. Spatial prediction of rainfall-induced landslides for the Lao Cai area (Vietnam) using a hybrid intelligent approach of least squares support vector machines inference model and artificial bee colony optimization. Landslides 14, 447–458.
Troiani, F., Della Seta, M., 2008. The use of the stream length–gradient index in morphotectonic analysis of small catchments: a case study from Central Italy. Geomorphology 102, 159–168.
Übeyli, E.D., Cvetkovic, D., Holland, G., Cosic, I., 2010. Adaptive neuro-fuzzy inference system employing wavelet coefficients for detection of alterations in sleep EEG activity during hypopnoea episodes. Digit. Signal Proc. 20, 678–691.
Vekaria, K., Clack, C., 1998. Selective crossover in genetic algorithms: an empirical study. In: Eiben, A.E., Bäck, T., Schoenauer, M., Schwefel, H.-P. (Eds.), Parallel Problem Solving from Nature — PPSN V: 5th International Conference Amsterdam, The Netherlands September 27–30, 1998 Proceedings. Springer, Berlin Heidelberg, Berlin, Heidelberg, pp. 438–447.
Wali, W.A., Al-Shamma'a, A.I., Hassan, K.H., Cullen, J.D., 2012. Online genetic-ANFIS temperature control for advanced microwave biodiesel reactor. J. Process Control 22, 1256–1272.
de Walque, B., Degré, A., Maugnard, A., Bielders, C.L., 2017. Artificial surfaces characteristics and sediment connectivity explain muddy flood hazard in Wallonia. Catena 158, 89–101.
Wang, Z., Lai, C., Chen, X., Yang, B., Zhao, S., Bai, X., 2015. Flood hazard risk assessment model based on random forest. J. Hydrol. 527, 1130–1141.
Ward, P.J., Jongman, B., Salamon, P., Simpson, A., Bates, P., De Groeve, T., et al., 2015. Usefulness and limitations of global flood risk models. Nat. Clim. Chang. 5, 712–715.
Winsemius, H.C., Aerts, J.C.J.H., van Beek, L.P.H., Bierkens, M.F.P., Bouwman, A., Jongman, B., et al., 2016. Global drivers of future river flood risk. Nat. Clim. Chang. 6, 381–385.
Xiao, Y., Yi, S., Tang, Z., 2017. Integrated flood hazard assessment based on spatial ordered weighted averaging method considering spatial heterogeneity of risk preference. Sci. Total Environ. 599, 1034–1046.
Xu, Y., Chung, S.-L., Jahn, B.-M., Wu, G., 2001. Petrologic and geochemical constraints on the petrogenesis of Permian–Triassic Emeishan flood basalts in southwestern China. Lithos 58, 145–168.
Yates, D.N., Warner, T.T., Leavesley, G.H., 2000. Prediction of a flash flood in complex terrain. Part II: a comparison of flood discharge simulations using rainfall input from radar, a dynamic model, and an automated algorithmic system. J. Appl. Meteorol. 39, 815–825.
Yesilnacar, E., Topal, T., 2005. Landslide susceptibility mapping: a comparison of logistic regression and neural networks methods in a medium scale study, Hendek region (Turkey). Eng. Geol. 79, 251–266.
Youssef, A.M., Pradhan, B., Hassan, A.M., 2011. Flash flood risk estimation along the St. Katherine road, southern Sinai, Egypt using GIS based morphometry and satellite imagery. Environ. Earth Sci. 62, 611–623.
Yu, F., Chen, Z., Ren, X., Yang, G., 2009. Analysis of historical floods on the Yangtze River, China: characteristics and explanations. Geomorphology 113, 210–216.
Zhang, Y., Smith, J.A., 2003. Space–time variability of rainfall and extreme flood response in the Menomonee River Basin, Wisconsin. J. Hydrometeorol. 4, 506–517.
Zolfani, S.H., Esfahani, M.H., Bitarafan, M., Zavadskas, E.K., Arefi, S.L., 2013. Developing a new hybrid MCDM method for selection of the optimal alternative of mechanical longitudinal ventilation of tunnel pollutants during automobile accidents. Transport 28, 89–96.
Zong, Y., Chen, X., 2000. The 1998 flood on the Yangtze, China. Nat. Hazards 22, 165–184.
Zorlu, H., 2017. Optimization of weighted myriad filters with differential evolution algorithm. AEU Int. J. Electron. Commun. 77, 1–9.